Effects of Zinc Concentration and Initial Condition on Precipitation Kinetics of Magnesium Alloys

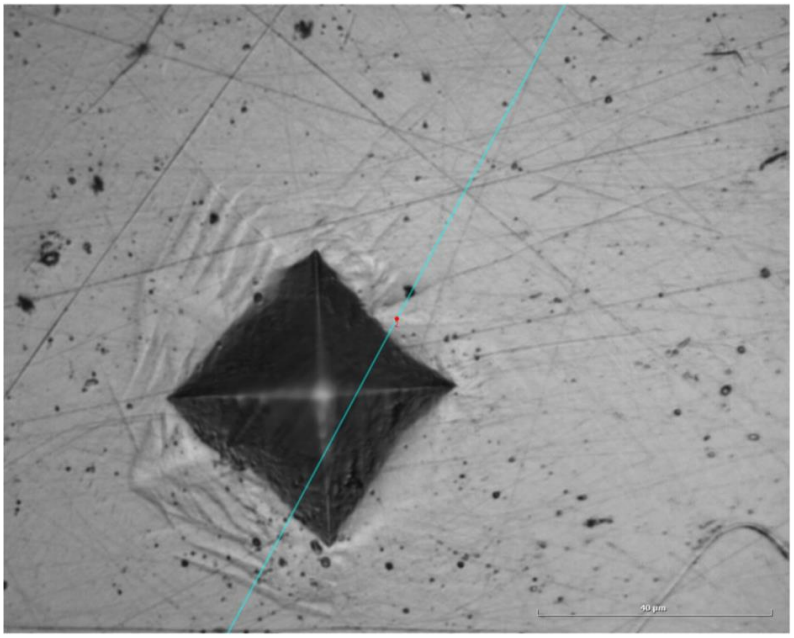

Marius Yuku

Division of Mechanics, Materials and Component Design

Department of Mechanical Engineering Sciences

Master Thesis 2024

CODEN:LUTMDN/(TMMV-5360)/1-63/2024

LUND UNIVERSITY | LTH FACULTY OF ENGINEERING

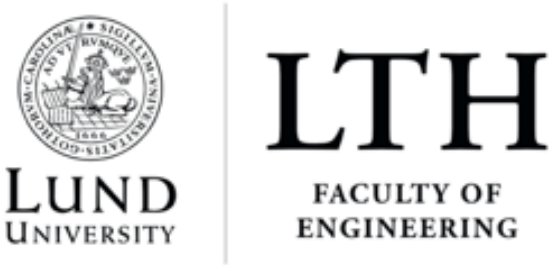

Effects of Zinc Concentration and Initial Condition on Precipitation Kinetics of Magnesium Alloys

Master Thesis

by

Marius Yuku

Division of Mechanics, Materials and Component Design

Department of Mechanical Engineering Sciences

Lund University 2024

Examiner: Filip Lenrick

Supervisor: Johan Ranstad

Co-Supervisor: Professor Dmytro Orlov

Division of Mechanics Material and Component Design
Department of Mechanical Engineering Sciences, LTH
Ole Römers väg 1
P.O. Box 118
SE-221 00, Lund, Sweden

Acknowledgements

Firstly, I would like to express my sincere gratitude to my supervisors Johan Ranstad and Dmytro Orlov for their invaluable guidance, support and encouragement throughout the process of completing this thesis. Their expertise and mentorship have been instrumental in shaping this research.

Secondly, I would like to thank my examiner Filip Lenrick for his insightful feedback and constructive criticism which subsequently greatly contributed to the quality of this work.

Thirdly, special thank to Agathi Dimakopoulou for her collaboration and assistance throughout this project.

I would also like to acknowledge my supporting friends and the equipment provided from the department of Lund University which made this research possible.

Finally, I extend my heartfelt thanks to my family who have supported me along the way. I am deeply indebted to them for their unwavering love, encouragement and understanding throughout my academic journey. Their support has been the cornerstone of my success.

Abstract

Magnesium alloys are promising candidates for biomedical implants due to their ability to dissolve in the human body, which improves the surgical procedures making a secondary surgery to remove the implant unnecessary. However, one of the main challenges magnesium alloys faces in terms of an implant is their inferior strength compared to such permanent implant materials as stainless steel and titanium.

In this work, Mg-Zn based alloys of high, medium and low zinc quantities and different processing states, homogenized and extruded, were heat treated to find peak aging time, which optimizes materials strength. During aging, the specimens were periodically extracted, and hardness tested to follow the process kinetics. It has been found that both the quantity of Zn in the Mg alloys, and processing state have significant impact on both aging kinetics and maximum hardness level at peak aging.

Furthermore, the specimen microstructure was studied with SEM to analyze grain sizes and intermetallic particle structure. Grain sizes were determined by linear intercept method. Homogenized material showed bigger grain size and lower quantities of particles compared to the extruded samples.

Keywords: Magnesium, Zinc, Mg-Zn alloys, precipitates, hardness, morphology, HCP, SEM, grain boundary, extrusion, homogenization, aging, peak aging, kinetics, temperature

Sammanfattning

Magnesiumlegeringar är lovande kandidater för biomedicinska implantat på grund av deras förmåga att lösas upp i människokroppen, vilket förbättrar de kirurgiska procedurerna och gör en sekundär operation för att avlägsna implantatet onödig. En av de största utmaningarna som magnesiumlegeringar står inför när det gäller ett implantat är dock deras sämre styrka jämfört med sådana permanenta implantatmaterial som rostfritt stål och titan.

I detta arbete värmebehandlades Mg-Zn-baserade legeringar av höga, medelhöga och låga zinkkvantiteter och olika bearbetningstillstånd, homogeniserade och extruderade för att hitta toppåldringstid, vilket optimerar materialstyrkan. Under åldrandet extraherades proverna periodiskt och hårdheten testades för att följa processkinetiken. Det har visat sig att både kvantiteten Zn i Mg-legeringarna och bearbetningstillståndet har betydande inverkan på både åldringskinetik och maximal hårdhetsnivå vid toppåldring.

Dessutom studerades provets mikrostruktur med SEM för att analysera kornstorlekar och intermetallisk partikelstruktur. Kornstorlekar bestämdes med linjär skärningsmetod. Homogeniserat material visade större kornstorlek och lägre mängd partiklar jämfört med de extruderade proverna.

Nyckelord: Magnesium, Zink, Mg-Zn-legeringar, fällningar, hårdhet, morfologi, HCP, SEM, korngräns, extrudering, homogenisering, åldring, toppåldring, kinetik, temperatur

Populärvetenskaplig sammanfattning

Magnesium är en silvervit metall med unika egenskaper som gör den väldigt intressant. Metallen är bland de lättaste med en densitet på 1.74 g/cm^3, återvinningsbar och leder ström. Magnesium är biologiskt nedbrytbart i kroppen och anses därmed vara en utav de främsta kandidaterna för biomedicinska implantat. En utav utmaningarna med användning av magnesium som implantat är dess begränsande inneboende mekaniska egenskaper som styrka och hårdhet. Magnesium och dess legering uppvisar lägre hårdhet jämfört med andra biomedicinska implantat som titan och stål. Numera används titan och stål för biologiska implantat, dessa material måste operareas ut efter läkemedelsprocessen vilket inte behöver göras för magnesium, vilket leder till att en sekundär operation inte skulle behövas genomföras. Ett område som har användning för förbättrad styrka och hårdhet av magnesium inom biologiskt implantat är de ortopediska, såsom skruvar och plattor som används för att fixera frakturer. Dessa måste utstå mekaniska påfrestningar samtidigt som de integrerar med kroppsvävnader. Slitstyrkan är direkt korrelerad till hårdhet och i biomedicinska implantat genererar högre hårdhet minskat slitage vid upprepad kontakt med andra kroppsdelar. Magnesium baserat implantat med optimerad hårdhet skulle innebära minskade hälsorisker och kostnader med tanke på materialet kan lösas upp i regereningsprocessen.

Innan tillämpningen av magnesium som implantat verkställs måste styrkan och hårdheten för implantatet optimeras. Detta görs med hjälp av en värmebehandlings process där magnesium åldras under en viss tid fram tills att högsta åldrandet är hittad, tidigare forskning har visat att Mg-Zn legeringar åldras mest utav alla Mg-legeringar. Åldrande är en värmebehandlingsmetod där Mg-Zn legeringar upphettas i en specifik temperatur och långsamt kyls ned. Denna process förändrar legeringens mikrostruktur vilket förbättrar dess mekaniska egenskaper.

I detta arbete genomgår Mg-Zn-legeringar av olika legeringssammansättning av hög-, medel- och låg zink tillsammans med olika bearbetningssteg, homogeniserade och extraherade åldringsvärmebehandling för att hitta toppåldring som optimerar materialens styrka och hårdhet, vidare studeras materialets ytmorfologi. Materialets hårdhets fås med hjälp av en hårdhetstest där hårdheten mäts varje timme efter åldring, denna undersökning utgör den största delen av arbetet.

Med zink som en legeringskomponent till magnesium förbättras dess styrka och hårdhet utan att vikten komprimeras. Anledningen är att zinkatomerna förvränger magnesiumgittret och hindrar dislokation rörelser som följaktligen ger upphov till ett starkare material. Under höga temperaturer accelereras fällningarna samtidigt som de blir grövre. Tiden spelar en viktig roll i åldringsprocessen eftersom längre tider eventuellt kan leda till överåldring. Detta fenomen resulterar i övervuxna fällningar, vilket minskar effektiviteten i att hindra dislokationer och minskar legeringshållfastheten. Kinetiken hos zink påverkar åldringsprocessen direkt. Åldringskinetiken är snabbare vid förhöjd temperatur där toppåldringen nås snabbare i jämförelse till lägre temperaturer. Vid temperaturer under 149 °C härdar G.P-zoner legeringen efter långa åldringstider. Men vid åldringstemperaturer över 149 °C bildar Mg-Zn-stavar en härdande fällningen och åldras därmed snabbare.

Glossary and abbreviations

Ar:	Argon
BSE:	Backscattered electrons
Ca:	Calcium
CRSS:	Critical Resolved Shear Stresses
Cu:	Copper
DP:	Diamond Polishing
EDS:	Energy- Dispersive X-ray spectroscopy
Fe:	Iron
HCP	Hexagonal Close Packed
Mg:	Magnesium
Mg-Zn:	Magnesium-Zinc
Mm:	Milimeter (unit: $1 \cdot 10^{-3}$ m)
MD DAC:	MultiDirectional Abrasive Cutting
MD MOL:	MultiDirectional Polishing with Molecular
MD NAP:	MultiDirectional Polishing with Nap Cloth
Na:	Natrium
Ni:	Nickel
O:	Oxygen
SEM:	Scanning Electron Microscope
SE:	Secondary electrons
SiC	Silicon Carbide
SSSS	Supersaturated solid solution
µm:	Micrometer (unit: $1 \cdot 10^{-6}$ m)
wt.%:	Weight percentage
Zn:	Zinc
Zr:	Zirconium

List of figures

Figure 1: Mg-Zn Binary phase diagram (Clark et al., 1988). 4
Figure 2: Steps of age hardening (Soboyejo, 2002).....8
Figure 3: Age hardening of Mg-5 wt.% Zn alloy (Clark,1965).....9
Figure 4: As casted with solid precipitates (left). Homogenized composition (right) (Viklund,2019).....10
Figure 5: SEM arrangement a) and incident electron beam and specimen b) (Goldstein et al., 2003). 12
Figure 6: Ejected electrons leading to inner-shell vacancies. Outer-shell electrons fills the vacancies and emits X-rays (Goldstein et al., 2013).....13
Figure 7: Side-view a) and top-view b) for the shape of Vickers indentation (Hegazy et al., 2023). 13
Figure 8: Specimen overview. 15
Figure 9 : : Oil bath One-7 by Memmert and personal protective equipment used in the experiments. 16
Figure 10: Cutting machine Struers Accutom-5 used in the experiments. 17
Figure 11: Selection guide for cutting wheels (Sturers, 2024). 17
Figure 12: Grinding equipment for specimen preparation used in the experiments. 18
Figure 13: Photograph of a semi-automated grinding/Polishing machine Struers Rotopol-2 used in the experiments. 19
Figure 14: Hardness test machine Struers Duramin 40 AC used in the experiments. 19
Figure 15: Angle distance of 11°and indentation distance of 200 μm. 20
Figure 16: SEM FEI Quanta 200 MKII instrument used in this work.....20
Figure 17: Etching machine, Gatan Model 682 (PECS) used in the experiments. 21
Figure 18: Indentations at different aging time. A) 0 hours, b) 7 hours, c) 17 hours and d) 25 hours. 22
Figure 19: Diagram showing the dependence of Vickers Hardness (HV) on time for Mg high Zn alloy in homogenized condition. Dots indicate experimental measurements, while dashed line show polynomial fitting. Peak aging is indicated with red line. 23
Figure 20: Indentations at different aging times. A) 0 hours, b) 7 hours, c) 18 hours and d) 25 hours. 24
Figure 21: Diagram showing the dependence of Vickers Hardness (HV) on time for Mg medium Zn alloy in homogenized condition. Dots indicate experimental measurements, while dashed line show polynomial fitting. Peak aging is indicated with red line. 24
Figure 22: Indentations at different aging times. A) 9 hours, b) 7 hours, c) 18 hours and d) 25 hours. 25
Figure 23: Diagram showing the dependence of Vickers Hardness (HV) on time for Mg low Zn alloy in homogenized condition. Dots indicate experimental measurements, while dashed line show polynomial fitting. Peak aging is indicated with red line. 26
Figure 24: Indentations at different aging times. A) 0 hours, b) 7 hours c) 8 hours and d) 18 hours. 27
Figure 25: Diagram showing the dependence of Vickers Hardness (HV) on time for Mg high Zn alloy in extruded condition. Dots indicate experimental measurements, while dashed line show polynomial fitting. Peak aging is indicated with red line. 27
Figure 26: Indentations at different aging times. A) 0 hours, b) 7 hours, c) 13 hours and d) 18 hours. 28

Figure 27: Diagram showing the dependence of Vickers Hardness (HV) on time for Mg medium Zn alloy in extruded condition. Dots indicate experimental measurements, while dashed line show polynomial fitting. Peak aging is indicated with red line. 29
Figure 28: Indentations at different aging times. A) 0 hours, b) 7 hours, c) 14 hours and d) 18 hours. 30
Figure 29: Diagram showing the dependence of Vickers Hardness (HV) on time for Mg low Zn alloy in extruded condition. Dots indicate experimental measurements, while dashed line show polynomial fitting. Peak aging is indicated with red line. 30
Figure 30: Summary of homogenized hardness measurements. 31
Figure 31: Summary of extruded hardness measurements. 31
Figure 32: SEM images of Mg medium Zn homogenized. A) BSE-100x, b) BSE-200x, c) BSE-500x, d) BSE 1000x. 32
Figure 33: SEM images of MG medium Zn homogenized over aged. A) BSE-100x, b) BSE-500x, c) BSE-1000x, d) BSE 5000x. 33
Figure 34: SEM images of Mg high Zn extruded. A) BSE-100x, b) BSE 500x, c) BSE-100x, d) BSE-500x 34
Figure 35: SEM images of Mg high Zn extruded overaged. A) BSE-100x, b) BSE-500x, c) BSE-1000x, d) BSE-5000x. 35
Figure 36: SEM images of Mg low Zn extruded. A) BSE-100x, b) BSE-500x, c) BSE-1000x, d) BSE-5000x 36
Figure 37: SEM images of Mg low Zn extruded overaged. A) BSE-500x, b) BSE-5000x, c) BSE-800x, d) BSE-3000x. 37
Figure 38: EDS analysis of studied spots for Mg low Zn extruded. 37
Figure 39: Mg medium Zn homogenized line interception of grains. 41
Figure 40: Mg medium Zn homogenized grain boundary intercepts. 41
Figure 41: Overaged Mg medium Zn homogenized line interception of grains. 42
Figure 42: Overaged Mg medium Zn homogenized grain boundary intercepts. 42
Figure 43: Mg high Zn extruded line interception of grains. 43
Figure 44: Mg high Zn extruded grain boundary intercepts. 43
Figure 45: Overaged Mg high Zn extruded line interception of grains. 44
Figure 46: Overaged Mg high Zn extruded grain boundary intercepts. 44
Figure 47: Mg low Zn extruded line interception of grains. 45
Figure 48: Mg low Zn extruded grain boundary intercepts. 45
Figure 49: Overaged Mg low Zn extruded line interception of grains. 46
Figure 50: Overaged Mg low Zn extruded grain boundary intercepts. 46

Table of Contents

1. Introduction *1*
1.1. Overview **1**
1.2. Aims **2**

2. Background *3*
2.1. Magnesium and its alloys **3**
2.2. Biomedical Magnesium **5**
2.3. Deformation mechanism **6**
2.4. Aging process **6**
2.4.1 Solution heat treatment 7
2.4.2 Quenching 7
2.4.3 Aging 7
2.5. Effect of zinc content on aging **8**
2.6. Processing of Mg alloys **10**
2.6.1 Homogenization 10
2.6.2 Extrusion 10
2.7. Analytical methods **11**
2.7.1 Scanning Electron Microscopy 11
2.7.2 Vickers hardness test 13
2.7.3 Grain size analysis 14

3. Method and materials *15*
3.1. Material selection and processing **15**
3.1.1 Material description 15
3.1.2 Aging heat treatment 16
3.2. Specimen preparations **16**
3.2.1 Cutting procedure 16
3.2.2 Grinding procedure 17
3.2.3 Polishing procedure 18
3.3. Hardness testing procedure **19**
3.4. Scanning Electron Microscopy examination prpcedure **20**
3.4.1 Specimen preparation for SEM 21

4. Results *22*
4.1. Hardness test **22**
4.1.1 Homogenized hardness 22
4.1.2 Extruded hardness 26
4.2. Microstructure characterization **32**
4.2.1 Surface morphology 32
4.2.2 EDS analysis 37
4.3. Grain size analysis **41**

5. Analysis and discussion *47*
5.1. Hardness and peak aging **47**
5.2. Surface morphology **50**
5.3. Grain size analysis **53**

6. Conclusions *55*

7. Future work *56*

8. References *57*

Appendix 1 ..... *- 1 -*

1. Introduction

1.1. Overview

Magnesium is a silvery-white metal with a density of 1.74 g/cm^3 making it the lightest engineering metal, while also being recyclable along with the ability to exhibit good electrical and thermal conductivity. Magnesium is the fourth most common element in the world as a whole and makes up approximately 13% of the planets mass. Also, the metal is the eighth most abundant element in the earth crust thus making it applicable in various engineering fields (Polmear et al., 2017).

Magnesium is a biodegradable material that is considered as a strong candidate for biomedical implants. Magnesium-based implants are breaking the paradigm in biomaterial science to develop corrosion resistant metals. The approach of temporary metallic implants for cardiovascular, musculoskeletal and general surgery is continuously developing in the biomaterial field (Witte, 2015). Biomedical implants are categorized into two, permanent and biodegradable ones. The permanent ones have shown to cause inflammatory responses, which is a risk of concern. Due to this risk, biodegradable implants are more popular considering their ability to dissolve in the human body (Espiritu et al., 2022).

Present implants for bone fracture treatments are usually made of titanium alloys, non-degradable steel or degradable polymers. This subsequently leads to toxic particles being released once they degrade in the body. Furthermore, the downside of using titanium alloys or steels for bone treatments also relates to the high stiffness compared to the natural bone. An implant with a higher stiffness than the surrounding bone bears a load higher than the bone structure, this causes a decrease in local bone density, also referred to as stress shielding (Frost, 1994). However, magnesium and its alloys mechanical properties are like those of natural bone, leading to that the stress shielding can be neglected (Jiang et al., 2020).

One of the challenges magnesium faces as an implant for biomedical application is the one regarding their inherent mechanical properties such as hardness. Magnesium and its alloys have lower hardness compared to other metals like titanium and steels which are also used in biomedical applications. Implants must endure mechanical stresses while interacting with body tissues, which can become an obstacle for magnesium and its alloys due to its relatively low hardness. Wear resistance is directly correlated to hardness and in biomedical implants, higher hardness is usually desired since it reduces wear during repeated contact with other body parts (Kirland et al., 2014, Staiger et al., 2006 & Tan et al., 2021).

Therefore, a biodegradable magnesium alloy designed to optimize its hardness is of great importance. The second surgery to remove the temporary implant would be avoided which improves the surgical experience but also benefits the health while also reducing both the cost and risks.

Out of all its alloying elements, the magnesium-zinc alloy exhibits the most age hardening. The aging kinetics depends on the alloying composition and the alloying containing element. Above 100 °C, age-hardening occurs rapidly, this is due the material going from supersaturated solid solution to building precipitates in the form of elongated morphology.

Hence why, the aging kinetics and the temperature is of interest when the investigating how to optimize the hardness of the magnesium alloys (Buha, 2008).

This work employs the utilization of hardness tests and Scanning Electronic Microscopy to explore and study the effects of age hardening on magnesium-zinc alloys at an elevated temperature. This is carried out with the silicon oil bath set-up at the Department of Mechanical Engineering Sciences at LTH.

1.2. Aims

Study the kinetics of aging in Mg-Zn based alloys along with the maximum hardes achievable at specificed conditions depedning on

- Zinc concentration and time.
- Initial (as-supplied) material condition, i.e. homogenized and extruded.

2. Background

2.1. Magnesium and its alloys

Pure magnesium is obtained from sea water in chloride form and as dolomites in the earth crust. It easily chemically reacts to water, nitrogen, carbon di-oxide and oxygen. Magnesium is a soft and mechanically weak material with an ability to corrode and has poor wear resistance, this makes it unsuitable to use in many fields. Thus, significant efforts in combining magnesium together with different alloys to get desired mechanical properties to use in various applications have been made (Prasand et al., 2017, Esmaily et al., 2017).

Magnesium alloys shows excellent weight to strength ratio, damping vibration, stiffness, specific strength and dimensional stability, owing to their HCP crystal structure. This makes the magnesium alloys tailored for aerospace and automobile industries (Prasand et al., 2017).

ASTM (American Society for Testing and Materials) names magnesium alloys with numbers and letters to define its elements. The numbers indicate the alloying elements nominal composition in weight. % while the letter describes the alloying content. For instance, AZ91 referrers to aluminum (Al) and zinc (Zn) with 9% and 1 % weight respectively in total while the rest is magnesium, this alloy offers good strength and corrosion resistance. Some of the most common commercial magnesium alloys are Mg-Al, Mg-Al-Zn, Mg-Zn and Mg-Zn-Zr. The alphabetic ASTM codes for magnesium alloying element is listed in table 1 (Prasand et al., 2017).

Table 1: ASTM codes for magnesium alloying elements (Prasand et al., 2017).

ASTM Codes	Alloying element
A	Aluminum
B	Bismuth
C	Copper
D	Cadmium
E	Rare Earth
F	Iron
G	Magnesium
H	Thorium
J	Strontium
K	Zirconium
L	Lithium
M	Manganese
N	Nickel
P	Lead
Q	Silver
R	Chromium
S	Silicon
T	Tin
W	Yttrium
X	Calcium
Y	Antimony
Z	Zinc

Zinc is after aluminum the most common alloying element for magnesium alloys and plays a significant role in the human body, which is one the reasons why it has emerged as a promising candidate for biomedical applications for magnesium alloys (Jiang et al., 2020). Furthermore, zinc is vital in the human body since it is indispensable for numerous psychological processes including immune function, wound healing and neurological function. The overall health and well-being depend on maintaining adequate zinc level through dietary intake (Hambidge 2000).

Zinc is recognized of being one most effective solute atom in terms of increasing strength and exhibits the most age hardening when alloyed, owing to its distinct difference in atoms radius compared to magnesium and due to its wide range of solubility (Somekawa et al., 2006).

The Mg-Zn binary phase diagram is illustrated in figure 1. At the temperature of 325 °C, the maximum amount solubility of zinc is found at 6.2 wt.%. But, once the temperature decreases, only 1.6 wt.% zinc remains soluble and leads to a solid solution strengthening while excess of zinc will form intermetallic phases as precipitate particles in the solid solution. Moreover, these intermetallic precipitates (Mg_XZn_y) will influence the materials age hardening effect (Jiang et al., 2020).

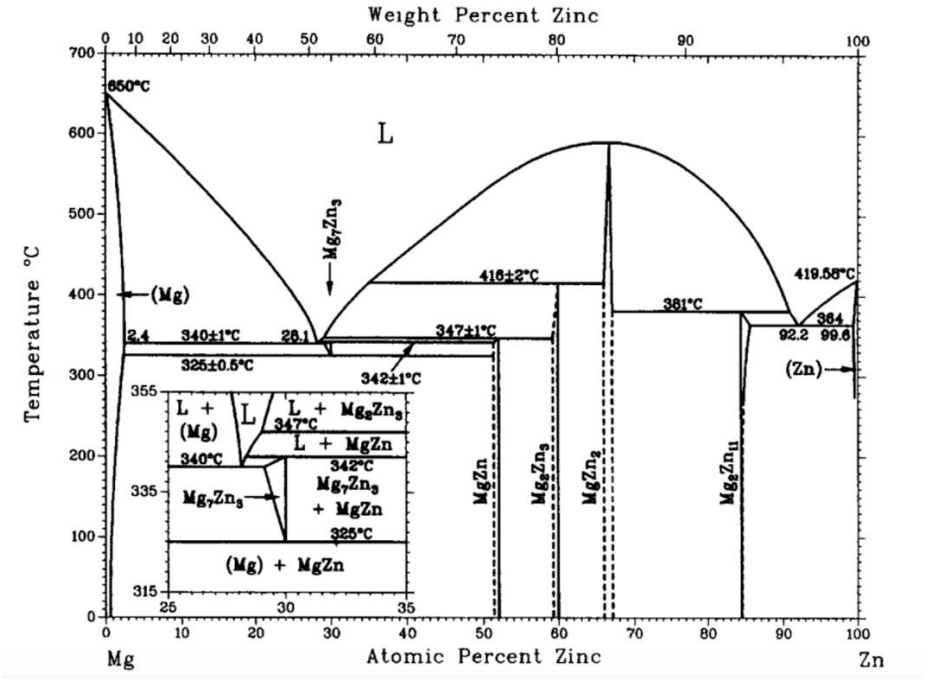

Figure 1: Mg-Zn Binary phase diagram (Clark et al., 1988).

As the zinc concentration increases towards 6.2 wt.%, the phase diagram may indicate the presence of additional phases, namely β-phase ($MgZn_2$) and η-phase (MgZn). The β-phase forms as the concentration of zinc increases. However, the η-phase forms at higher zinc concentrations, typically above 5 wt.%. These phases generally involve diffusion-controlled mechanism, with a changing alloy composition, the zinc atoms will diffuse within the magnesium lattice or form new intermetallic compounds. Nonetheless, the phase

transformation kinetics is affected by temperature and impurities (Okamoto et al., 1993, Du et al., 1999).

With the zinc as an alloying component to magnesium, its strength and hardness improves without compromising its weight. The reason is that the zinc atoms distort the magnesium lattice and hinders movement of dislocation which strengthens the material. Additionally, the Mg-Zn alloy can be further hardened with heat treatment process such as aging (Pekguleryuz et al., 2013).

This project will investigate Mg-Zn alloys with different zinc concentration from high zinc to low zinc within the region of 1.6 wt.% - 6.2 wt.% at a fixed elevated temperature of 180 °C to find the peak aging and its hardness, which requires the material to deform.

2.2. Biomedical Magnesium

Magnesium alloys are candidates for biomedical implants and have thereby extensively been studied. The material has unique set of mechanical properties, biocompatibility and biodegradability which gives it a promising potential in the medical field. Implants based on magnesium are breaking the paradigm in biomaterial science due to the continuous development of temporary cardiovascular, musculoskeletal and general implants for surgery (Witte, 2015). Nonetheless, magnesium most important ability is that it can resorb in the human body. This means that magnesium can dissolve in a biologically active medium without any effects which is an advantage, this result in eliminating a need for a second surgery to remove the implant after the healing process (Vinogradov et al., 2023). Therefore, magnesium is essential in a variety of physiological processes in the human body since it causes no harm when metabolized and extracted (Staiger et al., 2006).

Biomedical implants can be categorized into to permanent and biodegradable ones. Permanent orthopedic implant is prone to cause inflammatory responses and for this reason health risk is of concern. As a result to the health risks, biodegradable implants are more popular and suitable for surgery since they can dissolve in the human body (Espiritu et al., 2022).

The implants in orthopedic surgery and present bone fracture treatment are usually made of titanium alloys, non-degradable steel or degradable polymers. The downside of these material is the toxic particles released when degraded in the body. In addition, the mechanical properties of titanium and steel are not optimal since they have higher stiffness compared to the natural bone. When an implant has a stiffness higher than the surrounding bone, it leads to a decrease in the local bone density since the bone bears a load superior to the bone structure, this is called stress shielding (Frost, 1994). Conversely, the property of magnesium alloys is similar the natural bone (1.8–2 g/cm^3), this makes the stress shielding negligible (Jiang et al., 2020).

Although magnesium and is alloys have a prime advantage with reference to its biodegradability, the implants strongly benefit from the mechanical properties which include low density, low elastic modulus, corrosion resistance and high specific strength (Vinogradov et al., 2023).

However, one of the obstacles faced by magnesium and its alloys for biomedical application is their inherent mechanical properties, one of them being their hardness. Magnesium and its alloys have lower hardness compared to other materials like titanium and steel that also are

used in biomedical application. It is of vital importance that implants endures mechanical stresses when interacting with body tissues. This can become a challenge for magnesium alloys since its hardness is relatively low. Wear resistance is linked to hardness and is preferred in biomedical implants since higher hardness reduces wear when the implant is under repeated contact with other body parts (Kirland et al., 2014, Staiger et al., 2006 & Tan et al., 2021). Harder implant reduces the likelihood of material loss which can compromise the implants functionality. Also, hardness and strength contribute to dimensional stability of the implants, this make sure that the shape and structural integrity is maintained over time (Hermawan, 2012, Esmaily et al., 2017).

Mindful of this, a biodegradable magnesium alloy designed to optimize its hardness is important for the biomedical field. This reduces cost and risk since the second surgery to remove temporary implant can be avoided with biodegradable magnesium alloys.

There are already magnesium alloying implants commercially available and certified that can be found in companies, namely BIOTRONIK AG and Syntellix AG (BIOTRONIK AG, Syntellix AG). There is continuous ongoing research focalized at optimizing the properties of magnesium alloys and find prominent techniques to enhances their performance as implants (Jiang et al., 2020, Staiger et al., 2006, Vinogradov et al., 2023, Esmaily et al., 2017).

2.3. Deformation mechanism

Magnesium and magnesium alloys are anisotropic, meaning that their mechanical behavior varies with the direction once it deforms. In a particular crystallographic direction, the changes in the dimensions with temperature may not necessary be uniform. Anisotropic materials are strongly dependent on directions due to their variates in the periodicity and atom packing, this is due to their HCP crystal structure (Smallman et al., 1999).

During deformation of magnesium and magnesium alloys, single slip activates in one grain, this leads to movement of dislocations and the grain boundary acts as an obstacle to this motion. The dependence of temperature once different deformation mechanism is activated induces operating slip and twining (Mandia, 2018). At room temperature, the deformation of magnesium is limited due to limited number of slip and twining systems where the predominant slip mechanism is basal slip. However, at elevated temperatures the mechanical behavior of magnesium alloys is affected by the slip systems, the CRSS (Critical Resolved Shear Stresses) for non-basal slip system decreases as the temperatures increases. The reduced CRSS is caused by increased atomic mobility which facilitates the resistance towards dislocation motion across different planes in the crystal lattice (Chapuis et al., 2011). Besides the deformation by slip, another important deformation mechanism in HCP metals is deformation twinning. The interatomic distance in the magnesium lattice is relatively large combined with the low stresses between slip planes and large burger vector will facilitate twinning. Formed twin deformation either grow or shrink under shear stress and generates a change in shape and orientation. The most common twin boundaries in magnesium are the $\{10\bar{1}2\}$ slip plane in the $< 1011 >$ slip direction (Kaya et al., 2005).

2.4. Aging process

The heat treatment process that increases the hardness and strength of metal alloys by formation of very small, dispersed particles of a second phase within the original phase matrix, achieved by phase transformations that includes heat treatment is referred to as age hardening. This is due to the developing strength with time or as the alloy ages which is emphasized during the time-dependent aspect of the process. However, the same process is

also known as precipitation hardening, this highlights the hardening mechanism, particularly the precipitate formation which are the main contributors to the increased hardness (Callister et al., 2018).

The requisites for age hardening to take place is that there needs to be an appreciable maximum amount of solubility of a certain component in the other of several percent, such as zinc in magnesium, see figure 1. Also, the other condition that needs to be met is that the solubility limit need to decrease in the alloying element concentration with a decreasing temperature (Callister et al., 2018).

The age hardening process consist of three steps namely, solution heat treatment to dissolve soluble phases, quenching to create a supersaturated solid solution (SSSS) and age hardening for precipitation of solute atoms (Soboyejo, 2002).

2.4.1 Solution heat treatment

Solution heat treatment is the initial step in the age-hardening process. In this step the Mg-Zn alloy is heated to a temperature below the melting point of the magnesium within a single-phase region and held for a certain amount of time until a homogenous solid solution is formed and complete dissolution of solute element is achieved. This step also reduces any segregation present in the original alloy. The aim of this heat treatment step is to put the precipitating element in solid solution (Henkel et al., 2001).

2.4.2 Quenching

The following step in the heat treatment aging process is quenching. This is generally carried out by quickly cooling the alloy to room temperature usually by water, oil or air in order to obtain supersaturated solid solution of solute atoms but also vacancies. The rapid cooling hinders dissolved element from precipitating out while keeping them in a metastable state. The best mechanical properties are correlated with the most rapid quench rate as it influences the formation of undesired phases, which can lead to a weakened material by distortion or cracking in the components. Hence why equilibrium between fast cooling and minimization of distortion is desirable when components are quenched (ASM, 1991, ASM et al., 1992).

2.4.3 Aging

In the third step called aging, the supersaturated solid solution is heated at a temperature just below the solvus temperature during a period where the distance diffusion of atoms is short. Considering that the supersaturated is at metastable state and decomposed, the extra zinc atoms diffuse to several nucleation site that leads to growth of precipitates. These precipitates are finely dispersed and hinders dislocation movement within the crystal last and thereby strengthens the alloy (Askeland et al., 2010). Furthermore, the aim of aging is to improve the strength by forming G.P zones and precipitating second phase particles from solid solution gained from the quenching process. Although there are two types of aging, natural aging and artificial aging, this project focalizes on artificial aging. Natural aging is when the heat treatable alloys exhibit age hardening after quenching at room temperature. Conversely, artificial aging is the result of applied elevated temperature to obtain desired precipitation (ASM, 1991).

With controlled aging temperature and time, one can customize the properties of the alloys to meet specific requirements, making them highly versatile in a diverse set of applications. The aforementioned steps regarding the age hardening are found in figure 2.

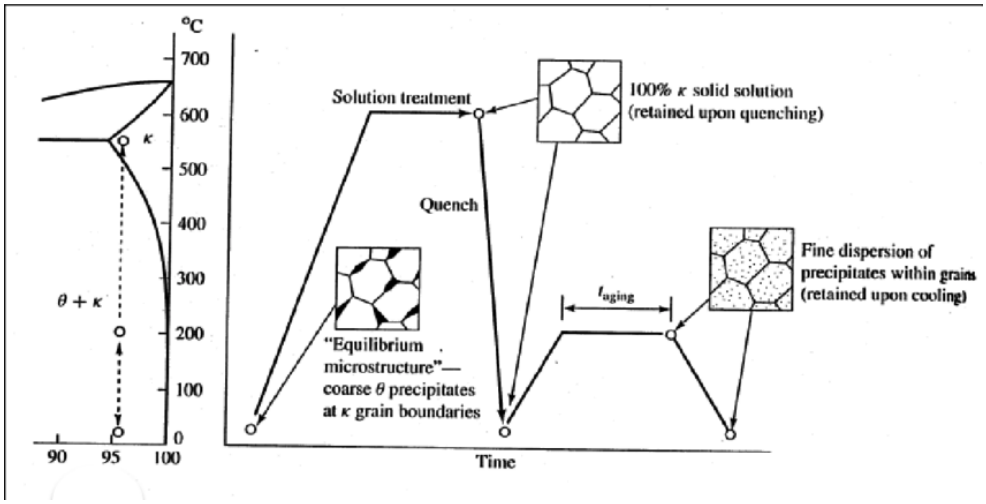

Figure 2: Steps of age hardening (Soboyejo, 2002).

The parameters affecting the aging process are temperature and time as shown in figure 2. At high temperatures, precipitates are accelerated but the precipitates are coarser, which result in a less effective alloy strengthening. The time play an integral part in the aging process since longer times can lead to over-aging. This phenomenon results to overgrown precipitates which reduces the effectives in hindering dislocation and decreases the alloys strength while also losing their coherency with the matrix. With increased time, the strength of hardness increases until a maximum and finally diminishes with reduction of hardness (Callister et al., 2018).

Before the over aging stage occurs, the peak aging condition has already been reached. This is characterized by the precipitates optimal size, distribution as well as coherence with the metal matrix while having the ability to block dislocation. The hardness increase during the aging and at the peak aged condition, the maximum hardness is attained (Geetha et al., 2015).

2.5. Effect of zinc content on aging

The kinetics of zinc directly impacts the aging process. Mg-Zn alloys in the composition range of 3-8 wt.% age hardenings between the temperature range of 70-260 °C. In the temperature range of 149 - 260 °C, the Mg-5 wt.% Zn alloy hardens by the precipitation of coherent transition lattice forming elongated morphology perpendicular to the basal plane. The aging kinetics are faster at elevated temperatures and peak aging is reached faster opposed to lower temperatures. However, at the lower temperatures the Mg- 5 wt.% Zn alloy result in higher hardness although longer aging time is required. At temperatures below 149 °C, G.P- zones harden the alloy after prolonged aging times. But, at aging temperatures above 149 °C, the Mg-Zn elongated morphology are the hardening precipitates (Clark, 1965).

Figure 3 displays the different age hardening of Mg-5 wt. % Zn alloy. As seen in this figure, the aging kinetics of rapid hardening is found at 149 °C and above, in contrast to 70 °C and 100 °C where hardening requires longer time. The Mg-5 wt.% Zn alloy peak ages to maximum hardness after 16 hours at the temperature 204 °C. The different response to aging temperature is due to the different precipitation process at 70 °C and 100 °C compared to transition lattice precipitation at 149 °C and above (Clark, 1965).

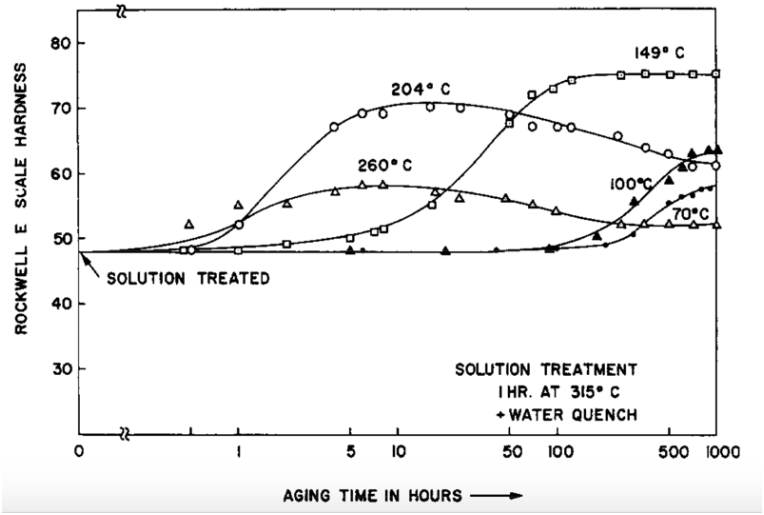

Figure 3: Age hardening of Mg-5 wt.% Zn alloy (Clark,1965).

The aging sequence always depends on the aging condition and the alloying concentration from a kinematic viewpoint. At Mg-4 wt.% Zn alloy, the aging sequence occurs rapidly above 100°C because of transition phases while requiring longer time below 100°C because of different G.P zones. The peak aging is found at 28 hours for the Mg-4 wt.% Zn at 185°C (Mima et al., 1971). The precipitates forming at elevated temperatures rely on the zinc composition and temperature. Regardless of the processing parameters, the enhancement of hardness that blocks dislocation movement are the microstructural characteristics of precipitates that usually are detected and that slides of the basal plane of the magnesium matrix in the Mg-Zn based alloys (Ren et al., 2021).

The hardness value of Mg-Zn alloys tends to be higher with containing higher zinc content, as is the case when highlighting the peak aging hardness at Mg-4 wt.% Zn compared to peak aging hardness at Mg-6 wt.% Zn when the temperature parameter is the same. Additionally, the peak hardness is acquired at an earlier time for the higher zinc content (Ren et al., 2021).

Age hardening at Mg-5.1 wt.% Zn alloy for 200°C leads to the occurrence of maximum hardness from 10 -50 hours. But, the peak aging is found at 28 hours while also showing very slow decrease in hardness after the peak was reached. This does not necessary indicate that stable precipitates were reached or that the transformation rate was slow. Nonetheless, at lower temperatures the strengthening is due to the cutting of smaller clusters of zinc by dislocation. The size and distribution of the zinc clusters depend on the concentration and the aging temperature. The clusters grow due to the zinc atom diffusion, which leads to growth of precipitates at elevated temperatures. In the Mg-5.1 wt.% Zn alloy composition, some clusters are expected based on the approximately 20% difference in atom size between magnesium and zinc (Chun et al., 1969).

Zn-rich precipitates can be considered as mechanism for strengthening the Mg-Zn alloy during aging since grain refinement, solid solution strengthening and precipitation hardening arise from the formation of zinc precipitates. Moreover, slow diffusion of the zinc element under the stage of grain growth leads to constitutional undercooling which then prevent the grains to grow. Additionally, smaller grains tend to strengthen the materials through grain boundaries (Asadollahi et al., 2020).

2.6. Processing of Mg alloys

2.6.1 Homogenization

Homogenization in magnesium alloys aims at obtaining uniform distribution of the alloying element and phases after casting. This is achieved by heat treatment process where different solid phase precipitate out and dissolve to the matrix. The magnesium alloy is heated above a critical temperature to reach a homogenized composition and is cooled afterwards (Liu et al., 2018). The homogenized magnesium alloys microstructure and morphology will differ from how it was as casted, see figure 4 (Viklund, 2019).

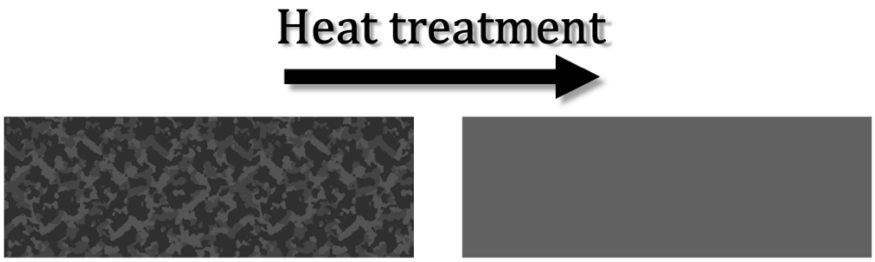

Figure 4: As casted with solid precipitates (left). Homogenized composition (right) (Viklund,2019).

The homogenization process scheme is important to determine beforehand to eliminate the casting segregation. Improvement in the composition segregation and structure segregation is necessary after a homogenized treatment (Liang et al, 2023). During casting, dendric structures and alloy segregation may exist and be particularly represented in heavy section. Considering that castings are not subjected to high temperature mechanical reduction and soaking treatments of wrought alloys, homogenizing the alloys is thereby required, particularly for aging. Homogenization prepares magnesium alloys for heat treatment by ensuring the effectiveness under the process. Uniform microstructures ensure more predictability and more consistent responses courtesy of the broken up structure to facilitate more consistent response to subsequent hardening (ASM, 1991).

However, in some cases during homogenized heat treatment for Mg-Zn alloys with 4.8-6.2 wt.% zinc, also referred to as ZK60, second phase compounds still exist between grain boundaries of the matrix while dendrites also show to exist. The reason behind this is the high content of zinc during casting. This causes non-equilibrium segregation, thus forms multiple number of secondary phases during solution. Furthermore, due to that zinc solubility in magnesium is high, solid solution decomposes under solidification and cooling, leavening room for precipitates and participles to exist in the matrix.
(Liang et al, 2023).

2.6.2 Extrusion

Extrusion is a common industrial process to create material with specific shapes and enhanced properties. This forming operation includes a metal bar being forced through a die by compressive force along with a reduced cross-sectional area (Callister et al., 2018). Microstructural parameters such a presence of second phase particles, grain size, texture and twins play a role in the hardness during and after the extrusion process. Besides, the alloying component and concentration are also crucial regarding the extrusion process. With higher zinc content, the process becomes more difficult due to the increasing hardness in the

material, consequently the extrudability decreases. It should be noted that lower zinc concertation to the magnesium result in better extrudability. Mg-Zn alloys with 3.8 wt.% zinc compared to 6.8 wt.% have a 3 times increased extrusion speed (Zeng et al., 2019).

During extrusion, the microstructure of the magnesium alloys changes significantly by undergoing severe plastic deformation attributed to changes in recrystallization, alignment of crystalline orientation such as basal texture, refinement of second phases and dynamic precipitation. The improved hardness after the extrusion process comes from enhancement in the grain boundary area that impedes dislocation motion. Moreover, extrusion aligns the grain along the extrusion direction (Tong et al., 2013). The alignment and texture not only lead to anisotropic behavior where the material exhibit strength which is the case for magnesium alloys since they usually have HCP crystal structures but also affect how the material deforms (Xu et al., 2012). The texture strongly impacts the mechanical behavior of the material, especially in the extrusion direction where the properties are enhanced (Tong et al., 2013, Zhang et al., 2011).

The distribution and size of the zinc containing precipitates can be altered during extrusion and another heat treatment method such as aging. After the material has been extruded and undergone aging, the supersaturated zinc atoms gradually precipitate out which creates coherent precipitates that blocks dislocation motion and therefore increases harness (Huang et al., 2013).

2.7. Analytical methods

The main analytical methods used in this project are Scanning Electron Microscopy (SEM), Vickers hardness test and grain size calculations.

2.7.1 Scanning Electron Microscopy

In this work, Scanning Electron Microscopy (SEM) is used to determine the microstructure and surface morphology of the specimens used before and after hardness deformation and heat treatment of aging. SEM is the most common type of electron microscope. SEM scans the surface of materials by using high resolution and larger depth of field. The images obtained by SEM are collected with the help of high energy focused electron beam scanning over the area of the specimen. This leads to multiple signals emitted from the specimens interaction volume. The optical arrangement of the SEM includes an electron gun, electromagnetic lenses, apertures and an electron detector that collects signals, presented in figure 5a). The signals can be categorized as backscattered electrons (BSE) and secondary electrons (SE) as presented in figure 5 b). When a contrast in the collected image appears, it entails that the beam aimed at the specimen varies with respect to different location throughout the surface. Once the electron beam impinges the specimen, multitude of signals are created, the most common ones are SE and BSE (Leng, 2013).

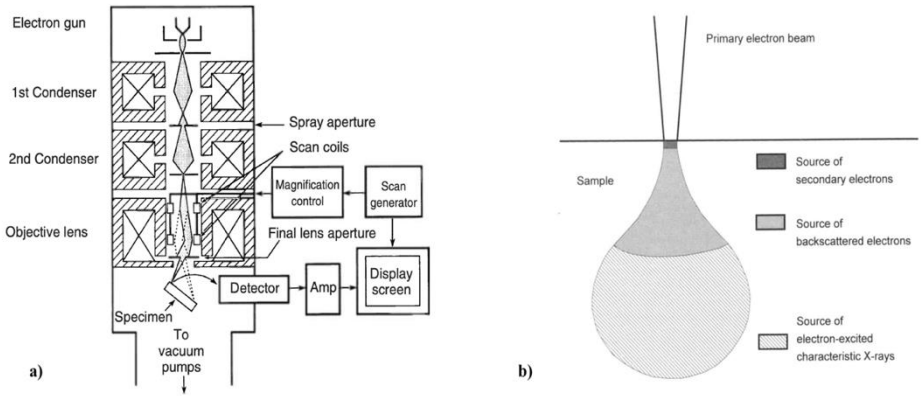

Figure 5: SEM arrangement a) and incident electron beam and specimen b) (Goldstein et al., 2003).

SE are known as secondary electrons which means that they get ejected by interaction with the primary beam electrons. SE have low energy and can thereby can escape only from a small region at the specimen surface. This leads to SE having the best imaging resolution. The imaging contrast comes from the surface topography. Moreover, the volume interaction is referred as the place signals originate and eventually escape to be detected. SE have more interactions closer to the surface which makes the electrons more prone to escaping, to point at the peak top instead to point at the valley bottom. The peaks are interpreted as bright while the valleys are interpreted as dark, correspondingly easy to interpret (Goldstein et al., 2003).

BSE are beam electrons that are scattered back out of the specimen with elastic collision along with nuclei specimen atoms. BSE have higher energy which leads to it having larger interaction volume thus have a limited imaging resolution. The contrast in the images mainly comes from point-to-point differences in the specimens average atomic number. Higher atomic number nuclei backscatter more electrons, this leads to brighter areas in the SEM imaging (Goldstein et al., 2003).

Due to zinc having a larger atomic number (30) compared to magnesium (12), the brighter regions in SEM imaging will be of the zinc material while the darker regions will be of magnesium material owing to the lower atomic number. Zinc appears brighter because of increased backscattered electron signal compered to magnesium since it has a stronger electron scattering (Philips,1996). SE are categorized as inelastic energy while BSE are categorized as elastic energy. Inelastic energy referrers to emission of the SE being ejected from the specimen when energy is transitioned from electron to specimen. However, elastic energy refers to high energy BSE and atomic nucleus giving rise to elastic scattering, meaning no to little energy being transferred from electron to specimen (Egerton, 2005).

Energy-Dispersive X-ray spectroscopy (EDS) is an analytical technique that identifies composition of element of material analysis in a solid state. The EDS system is mounted in the SEM where it uses the primary beam of the microscope with intention to generate characteristic X-rays. Analyzing the energy of these characteristic X-rays helps detect the specimen composition (Hollerith et al., 2004).

When the atom is exposed to ionizing radiation of high energy, the electrons get ejected which subsequently leads to the electrons leaving inner-shell vacancies, visualized in figure

6. The outer-shell electrons transition fills the vacancy spot and emits the X-rays, the energy is determined by the atoms energy, also visualized in figure 6. (Hare et al., 2015).

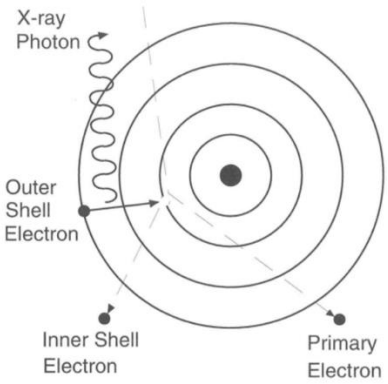

Figure 6: Ejected electrons leading to inner-shell vacancies. Outer-shell electrons fills the vacancies and emits X-rays (Goldstein et al., 2013).

Every material is unique and have a specific energy difference in their shells. The results from EDS analysis are usually presented in tables and diagrams that help to understand the composition of element in the specimen (Goldstein et al., 2003). Additionally, the X-ray spectrum that is emitted gives quantitative information regarding the elements in the specimen that is ionized by an incident radiation whereas focused incident beams and a detector are used to map the elements distribution at high spatial resolution (Hare et al., 2015).

2.7.2 Vickers hardness test

Vickers hardness testing is a method that determines the hardness of a material to deformation by using a 136° pyramidal diamond indentation to form square indentations on a specimen, presented in figure 7a) and figure 7b). The hardness scale is wide, making it suitable to test metals and welds (Hegazy et al., 2023).

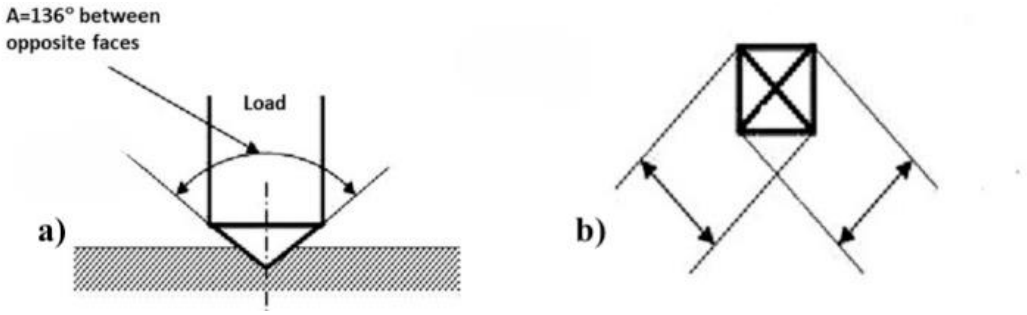

Figure 7: Side-view a) and top-view b) for the shape of Vickers indentation (Hegazy et al., 2023).

The load is applied for a duration of approximately 10-15s with two axes of the diamond shaped indentation, measured in millimeters and averaged which gives the dimension (d) so that the hardness can be determined based on different loads of calibration (P). The expression to calculate the Vickers hardness in found in equation 1. The load applied usually varies depending on the material being tested, this ranges from a few grams to several

kilograms. For instances, the hardness (HV) can be expressed as HV10 for a load of 10kg and HV5 for a load of 5 kg (Moore et al., 2015).

$$HV = 1.8544 \frac{P}{d^2} \quad (1)$$

This method will be applied before and after the heat treatment of the specimens to compare how the hardness have been affected during aging.

2.7.3 Grain size analysis

Determining the grain size is an applicable method to use when properties of polycrystalline or single-phase materials are considered. Every material has a variety of shape and size of distribution with regards to their constituent grains. Furthermore, the grain sizes may be specified as average or mean grain diameters. Although the approach to determine a grain size are multiple, this work focuses on the linear intercept method, which counts the number of grain boundary interception with the help of straight lines. These lines are randomly drawn through multiple photomicrographs showing the grain structure from the same magnification, the grain boundaries intersected by all the line segments are then counted. The parameters to calculate the grain size are expressed in equation 2. The sum of the total number of interceptions is defined as P and the total length of all lines is defined as LT. M is the magnification and the mean intercept length is defined as $\bar{l}$ *(*Callister et al., 2018).

$$\bar{l} = \frac{L_T}{PM} \quad (2)$$

The valuable information gathered from the grain size analysis will help to further understanding the material behavior before and after aging and to see how its mechanical properties in the context of grain size and hardness have changed.

Scale bars are typically used to indicate magnification degree. The scale bars in this report is a straight horizontal line expressed in microns located near the micrographic image. The value from the scale bar represents the distance on magnified space corresponding to the length in the scale. The following approach is generally used to compute magnification from a scale bar, firstly length of the scale bar is measured using a ruler. Secondly, the length is concerted into microns. For instance, if the measured scale length approximately is 10 mm, it would then be 10 000 μm. Thirdly, if the scale bar length is 100 μm, the magnification is calculated with the expression in equation 3.

$$M = \frac{Measured\ scale\ length\ (\ converted\ to\ microns)}{The\ number\ appearing\ by\ the\ scale\ bar\ (in\ microns)} \quad (3)$$

3. Method and materials

3.1. Material selection and processing

3.1.1 Material description

The company LBM Sweden AB provided magnesium alloys with varying zinc content categorized into high, medium and low zinc. Since zinc content and processing state influence the mechanical properties of the material, multiple specimens had to be prepared and labeled appropriately. Although there is appreciation that other alloying elements have effect on material properties, grain and precipitate structure evolution, they were not varied in the supplied set of samples, and therefore excluded from the scope of present study.

Nine specimens were prepared for high, medium and low Zn quantity and respective processing state of Mg alloys, i.e. homogenized and extruded. These specimens were then sub-divided, so that one heat treated to over aged state, four specimens peak aged (once respective condition was found), and the reminder remained as received. All the specimens were grinded and polished to various surface qualities depending on intended analysis, as described below.

Figure 8 summarizes the specimen availability, preparation and testing in a schematic diagram. In ageing heat treatment, specimens were extracted from the oil bath for hardness testing after every hour. Once the specimen reached peak aged condition, its microstructure was analyzed with SEM.

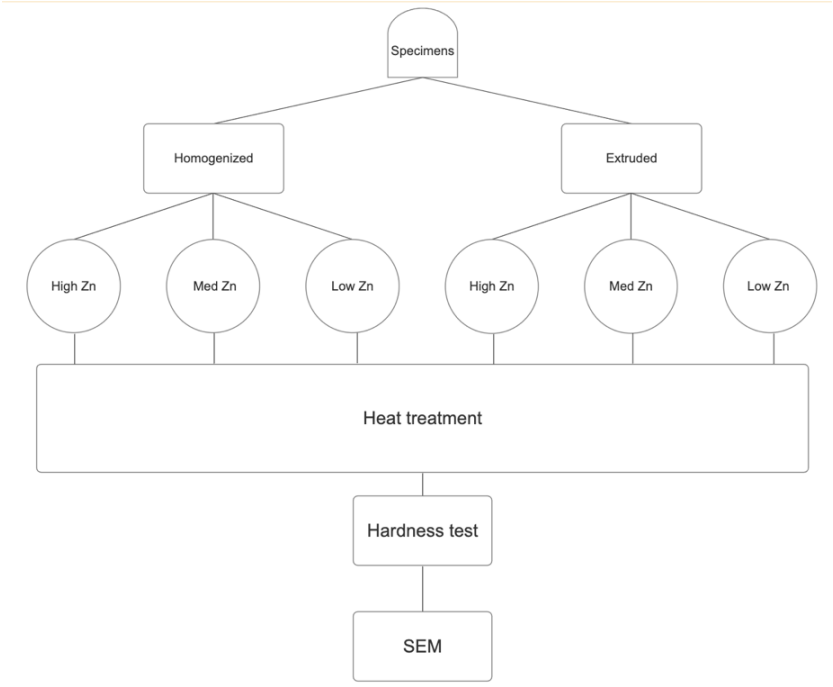

Figure 8: Specimen overview.

3.1.2 Aging heat treatment

Once the specimens had been grinded and polished to a surface quality appropriate for Vickers hardness testing, they were ready for aging in the silicon oil bath. Figure 9 shows the oil bath and the equipment used. Considering that the silicon oil tends not to evaporate and owing to the high temperature, heat-pretection gloves, appron and and full-face maskwere necessary to use. The specimens were placed in different test tubes that were labeled depending on specimen condition and placed in the oil bath at constant temperature of 180 °C. The oil bath used in this project was the ONE-7 by Memmert.

Figure 9 : Oil bath One-7 by Memmert and personal protective equipment used in the experiments.

The specimens were taken out the oil bath with a period of one hour for hardness testing until peak-aged condition was found.

3.2. Specimen preparations

Multiple steps had to be carried out to obtain specimen surface of sufficient quality. The procedures regarding the specimens preparation were carried out as described below.

3.2.1 Cutting procedure

Magnesium bars provided by the company named LBM consisted of different zinc concentrations and processing of Mg alloys which had to be cut into small and circular specimens with a diameter of 10 mm and a thickness of 2 mm. This was made possible by usinng the cutting machine Struers Accutom-5 composed by a wheel holder, cutting wheel and specimen holder that can rotate and move in x and y direction, see figure 10.

Figure 10: Cutting machine Struers Accutom-5 used in the experiments.

Considering that magnesium is of HCP crystal structure with limited available slip systems at room temperature and given that the material is non-ferrous, the recommended cutting wheel used was the SiC 10S15 from Struers, as illustrated in figure 11. The used cutting parameters were rotational speed of 3000 RPM and a feed speed om 0.1 mm/s.

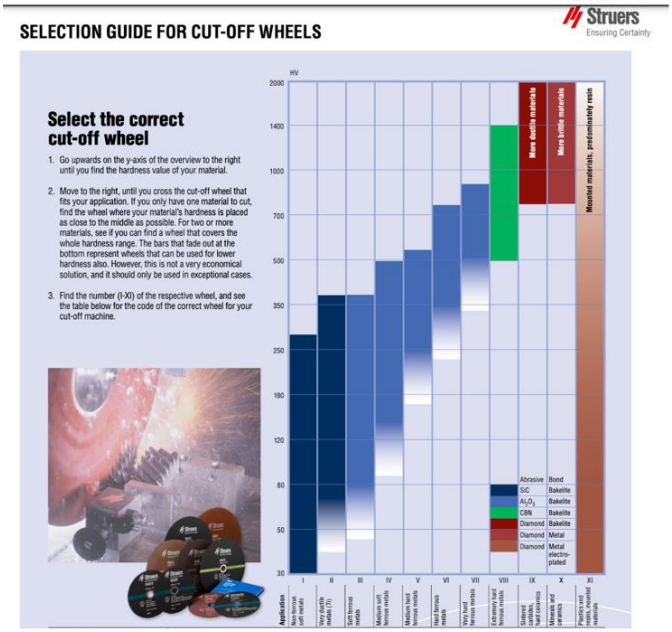

Figure 11: Selection guide for cutting wheels (Sturers, 2024).

3.2.2 Grinding procedure

The specimens were ground with SiC paper. The objective with the grinding is to achieve a homogenized surface free from deformation from the previous step. The specimens were ground on abrasive rolls with 4 different grit sizes moving from 360 grit to 600 grit, 800 grit and 1200 grit, as shown in figure 12.

Figure 12: Grinding equipment for specimen preparation used in the experiments.

The different grit size help with achieving a smooth surface. Between every grinding step, the specimens were washed with water then dried with compressed air. The specimens were cleaned with ethanol and dried with compressed air at the last wash. The reason behind this is so that the ethanol help preserve the specimen.

3.2.3 Polishing procedure

The purpose of polishing the specimens is to obtain a mirror-like surface where scratches and irregularities are removed without subsurface damage. The picture of used polishing machine Rotopol-2 can be found in figure 13. To achieve the mirror-like surface finish, polishing solution of DP-Suspension M3 µm and DP-Lubricant green along with polishing disc MD-Dac on magnetic wheel were used. Furthermore, after the specimen had been washed with water and dried with compressed air, DP-Suspension M1 µm and DP- Lubricant green was applied along with polishing disc MD-Mol. Once the specimen had been washed with ethanol, DP-Suspension A 1/4 µm and DP-Lubricant yellow was applied along with polishing disc MD-Nap. The DP-Suspensions contains abrasive particles that help remove all the imperfections and scratches on the surface. The different polishing disc MD creates more contrast between the different phases so that the requirement of different surface finish so that desired result during analysis is reached.

Figure 13: Photograph of a semi-automated grinding/Polishing machine Struers Rotopol-2 used in the experiments.

The specimens were taken out of the oil bath after one hour and went through hardness testing until the peak age was found.

3.3. Hardness testing procedure

The hardness testing was carried out using Vickers method available through Duramin 40 AC instrument, see figure 14.

Figure 14: Hardness test machine Struers Duramin 40 AC used in the experiments.

A representative indent specimen is presented in figure 15a). Every indentation series had an angle distance of 11° away from the previous one so that as many test series as possible could be made throughout the specimen surface, as displayed in figure 15b). The indentation

distance used was 200 μm which prevents one indentation from affecting the other once it has deformed the surface of the Mg-Zn alloy. The hardness machine used a 100 g indentation at a 10 s dwell time for 11 indentations that were averaged to achieve sufficient statistical representation. The indents were measured as magnifications ranging from 2.5-50x in compliance with ASTM E92-03 standard.

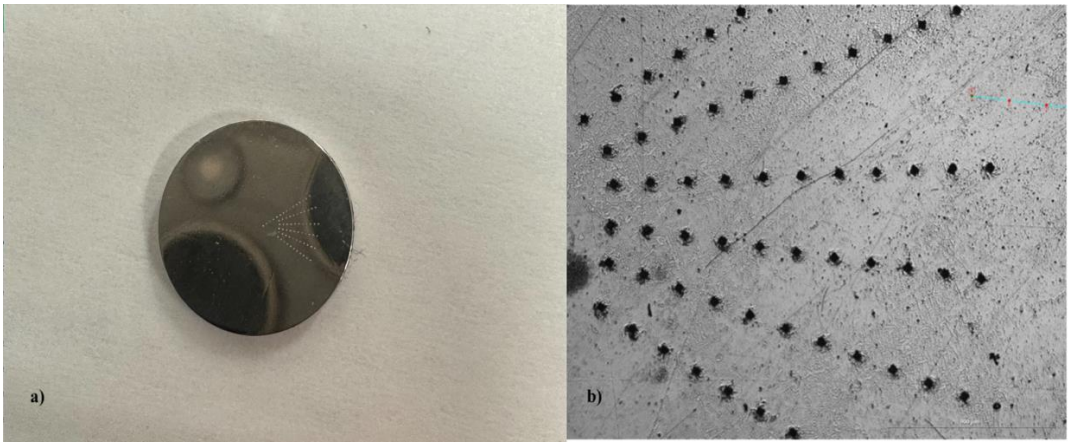

Figure 15: Angle distance of 11°and indentation distance of 200 μm.

3.4. Scanning Electron Microscopy examination prpcedure

Examining the microstructural state of the Mg-Zn alloy specimens to compare the changes from heat treatment aging and as received, was possible with SEM imaging in secondary and backscattered electrons. The used SEM instrument in figure 16 was FEI Quanta 200 MKII combined with EDAX EBSD+EDS system Pegasus. The magnification which was used ranges from 1000- 20k depending on microstructure features of interest. During the analysis of SEM imaging, it was important to indentify the concentrations elements in various locations, which was carried out with EDS analysis.

Figure 16: SEM FEI Quanta 200 MKII instrument used in this work

3.4.1 Specimen preparation for SEM

The final preparation step before SEM examination entailed precision broad ion-beam etching. The specimen was mounted on a specimen holder by a conductive carbon tape and then placed in the etching machine named Gatan Model 682 (PECS), see figure 17. A layer of the material gets removed, so that the underlying structure can be exposed by ion polishing system to prepare a high-quality specimen for SEM. The parameters used for the etching machine was a beam energy of 5kEV, the etching gun of around 270 μm, rotation angle of 20° and a timer of 5 minutes.

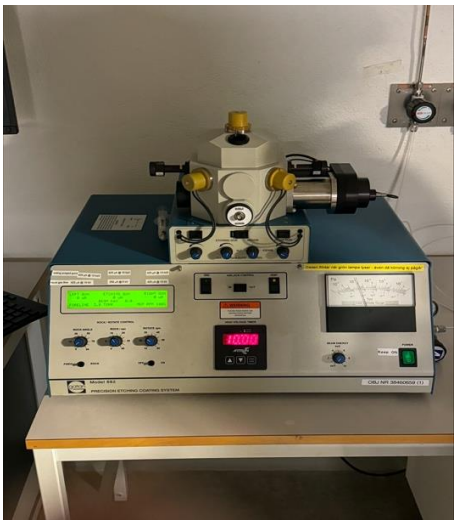

Figure 17: Etching machine, Gatan Model 682 (PECS) used in the experiments.

4. Results

The obtained experimental results are subdivided in two parts describing the hardness testing and then the microstructure analysis using SEM including EDS.

4.1. Hardness test

The Vickers hardness testing was carried out on specimens extracted periodically after every hour during aging at 180 °C silicon in a silicone oil bath resulted in the indentations penetrating the specimen surface which led to some interesting findings depending on the processing of Mg alloys and alloying zinc composition. The hardness test results are divided into two parts, homogenized and extruded.

4.1.1 Homogenized hardness

Figure 18 illustrates the indentation imprints and surface morphology of the homogenized high zinc alloy after different hour stages in the aging process. Figure 18a) presents the specimens initial hardness at 61.6 HV before it went through aging heat treatment. The figure 18a) shows the compressed results of the specimen where twinning deformation and basal slip of the Mg-Zn alloys can be found. Furthermore, figure 18a) also shows a homogenized surface. Figure 18b) is taken from the aging time of 7 hours with a hardness of 68.6 HV where the indentation deforming the specimen surface, evidently show more twin deformation. Figure 18c) is taken from 17 hours of aging which was the time when peak aging occurred for the homogenized high zinc alloy specimen with a peak hardness of 74 HV. Additionally, figure 18c) show a different deformation pattern. The figure 18d) is taken from 25 hours of aging, at this point the specimen had already been overaged and resulted in a hardness of 72.1 HV. The surface morphology shows some scratches, damages of corrosion but also some darker spots that could be precipitates. However, further investigation with SEM will confirm if the statement regarding the darker spots indeed is accurate of not.

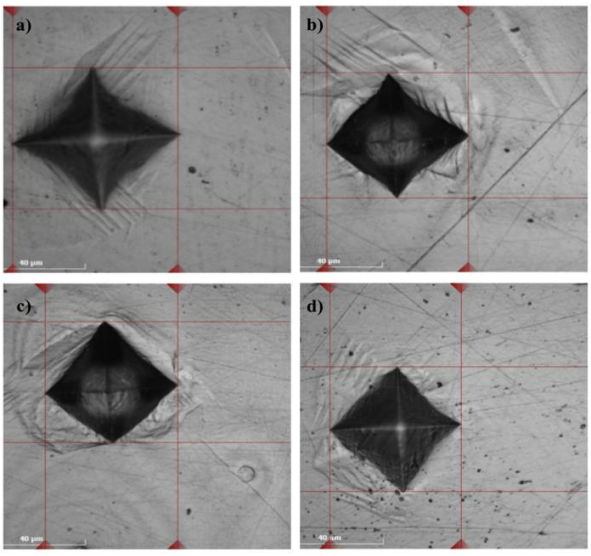

Figure 18: Indentations at different aging time. A) 0 hours, b) 7 hours, c) 17 hours and d) 25 hours.

Figure 19 illustrates the peak aging for the magnesium high zinc homogenized specimen. The plotted graph is a dashed line of third polynomial order with an expressed function found in figure 19 that best fits the collected data from the hardness test. The peak hardness is found at

74 HV at 17 hours of aging and was calculated by deriving the expressed function to a second order polynomial and then solving for it. The spread of dots are the hardness measurements during different time of aging.

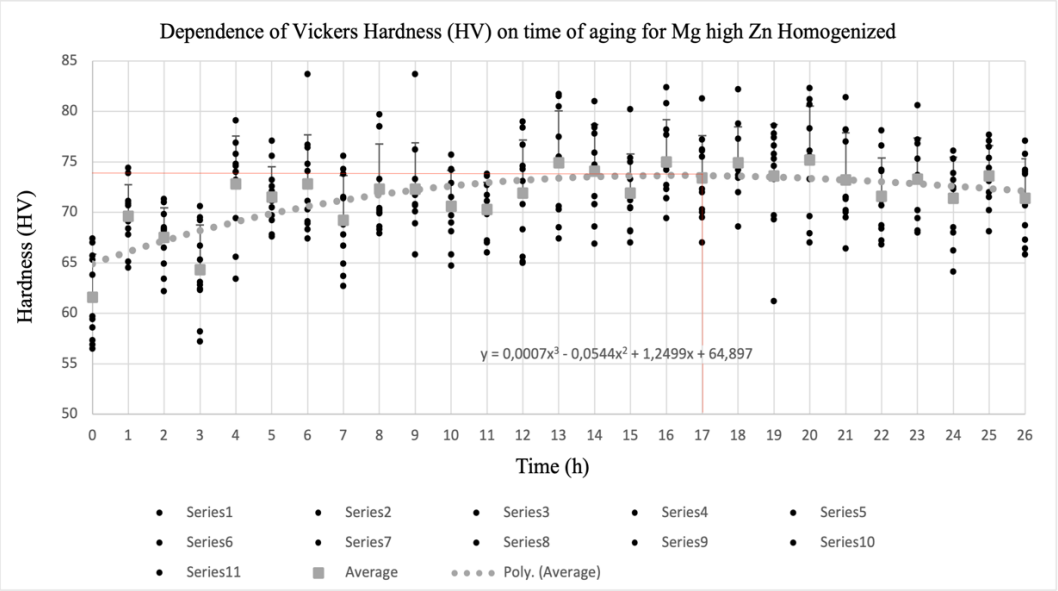

Figure 19: Diagram showing the dependence of Vickers Hardness (HV) on time for Mg high Zn alloy in homogenized condition. Dots indicate experimental measurements, while dashed line show polynomial fitting. Peak aging is indicated with red line.

Figure 20 shows overview of indentation imprints on the surface of the homogenized medium zinc specimen after aging for different times. The hardness before aging resulted in a hardness of 53.5 HV. The surface is homogenized and a visible deformation pattern is shown. Figure 20b) shows the hardness indentation from aging at 7 hours with a hardness of 63.5 HV, the texture is visibly shown and there are clear twins shown. Scratches from the grinding and polishing process are also visible. Moreover, the indentation in figure 20b) is somewhat asymmetrical and not like a square pyramid. Figure 20c) shows one of the indentations from the peak aging found at 18 hours with a hardness value of 70 HV. Deformation on the surface caused by the indentation from the hardness tester is also presented in figure 20c). The larger darker dots in figure 20d) are most likely corrosion due to environmental contact while the smaller dots possibly either could be impurities or precipitates. However, this will be validated with SEM. Deformation is clearly seen in the specimen nearby the indentation from figure 19d). Additionally, shown in figure 20d) is the specimen at an overaged stage of 25 hours and a hardness of 65.8 HV.

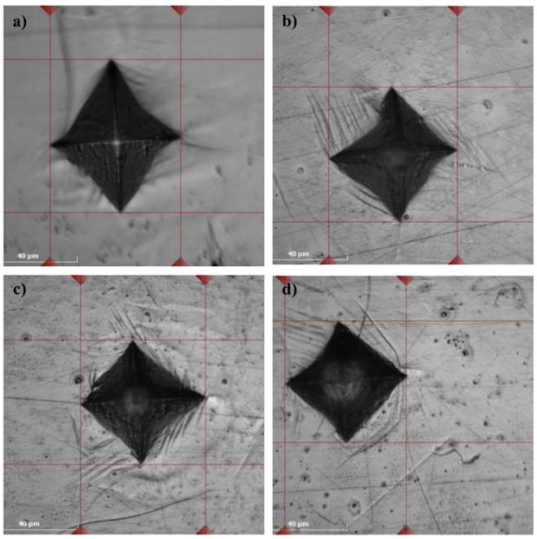

Figure 20: Indentations at different aging times. A) 0 hours, b) 7 hours, c) 18 hours and d) 25 hours.

Figure 21 presents the peak aging for the magnesium medium zinc homogenized specimen. The plotted graph is a dashed line of third polynomial order with an expressed function found in figure 21 that best fits the collected data from the hardness test. The peak hardness is found at 70 HV at 18 hours of aging and was calculated by deriving the expressed function to a second order polynomial and then solving for it. The spread of dots are the hardness measurements during different time of aging.

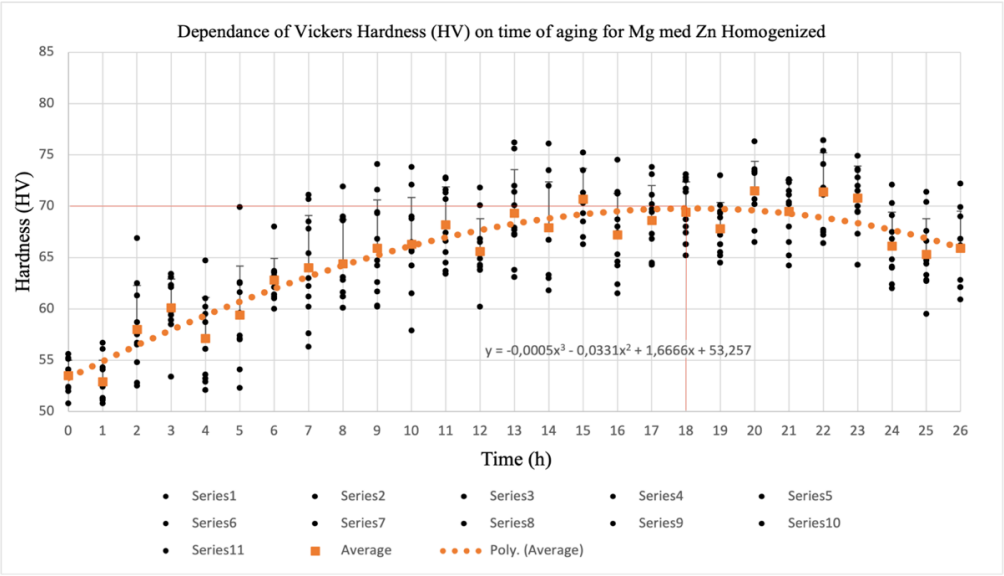

Figure 21: Diagram showing the dependence of Vickers Hardness (HV) on time for Mg medium Zn alloy in homogenized condition. Dots indicate experimental measurements, while dashed line show polynomial fitting. Peak aging is indicated with red line.

Indentation imprints of he homogenized low zinc concentration is illustrated in figure 22. The initial hardness before the specimen underwent aging was 63.8 HV. Figure 22a) shows a homogenized but deformed surface with an indentation where twins also are shown. The specimens hardness increases to 65 HV after 7 hours of aging, visible scratches from the

polishing and grinding process are visible along with the notable twins forming outside the indentationer, see figure 22b). The peak aging is found at 18 hours with a hardness of 68.6 HV, the different deformation patterns and twins are obvious, see figure 22c). The indentation in figure 22d) is from the over aged stage at 25 hours with a hardness of 67 HV where different twins are shown. However, the created twins in figure 22c) are apparent but there are also some darker spots in the surface morphology that needs to get verified with optical instrument.

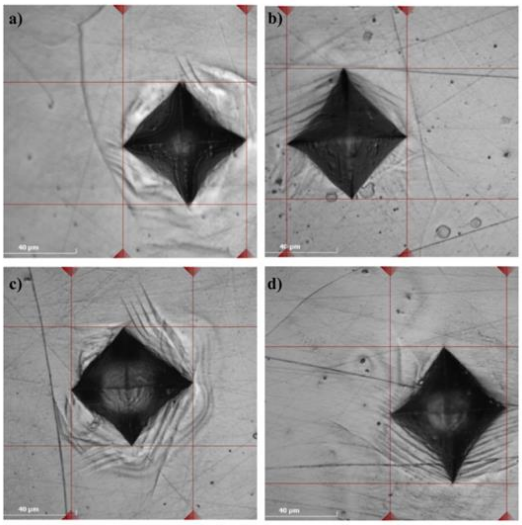

Figure 22: Indentations at different aging times. A) 9 hours, b) 7 hours, c) 18 hours and d) 25 hours.

Figure 23 shows the peak aging for the magnesium low zinc homogenized specimen. The plotted graph is a dashed line of third polynomial order with an expressed function found in figure 23 that best fits the collected data from the hardness test. The peak hardness is found at 68.6 HV at 18 hours of aging and was calculated by deriving the expressed function to a second order polynomial and then solving for it. The spread of dots are the hardness measurements during different time of aging.

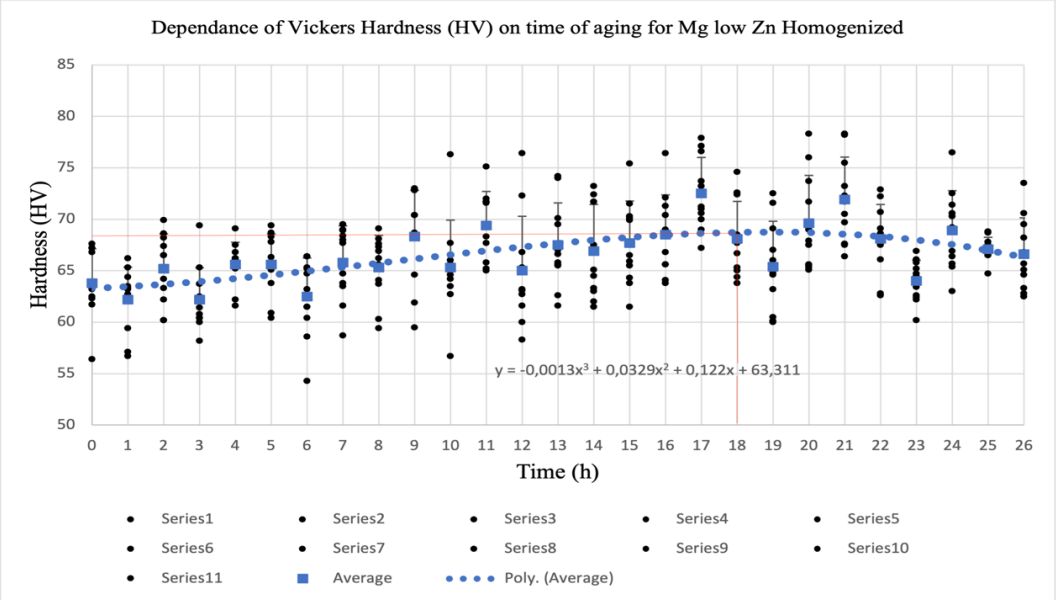

Figure 23: Diagram showing the dependence of Vickers Hardness (HV) on time for Mg low Zn alloy in homogenized condition. Dots indicate experimental measurements, while dashed line show polynomial fitting. Peak aging is indicated with red line.

4.1.2 Extruded hardness

Figure 24 presents the indentation imprints and surface morphology of the extruded high zinc alloy. The initial hardness before the aging heat treatment for the extruded specimen of high zinc content was 61.9 HV, the surface appears to already have a lot of darker spots before the aging and the deformation around the indentation is moderately apparent, see figure 24a). The indentation visible in figure 24b) is from aging at 7 hours which resulted in a hardness of 64.4 HV, the surface shows some darker spots throughout the surface and a slight deformation around the indentation. Figure 24c) is the indentation from the peak aged stage at 8 hours with a hardness of 65 HV where a more evident deformation is noticeable but also a couple of grain boundaries. Figure 24d) is from an indentation at 18 hours when where the specimen is at an overaged stage with a hardness of 63.7 HV. Whether or not the darker spots are dirt particles or precipitates, see figure 24d) will be confirmed with SEM. Furthermore, some silicon oil particles left after the specimen had been washed with ethanol and dried with compressed air is visible in figure 24d).

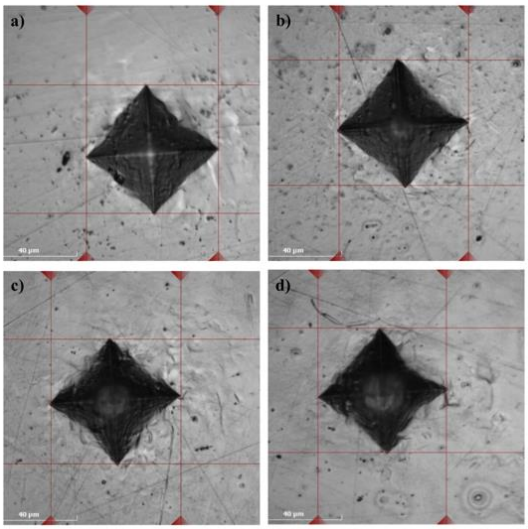

Figure 24: Indentations at different aging times. A) 0 hours, b) 7 hours c) 8 hours and d) 18 hours.

Figure 25 displays the peak aging for the magnesium high zinc extruded specimen. The plotted graph is a dashed line of third polynomial order with an expressed function found in figure 25 that best fits the collected data from the hardness test. The peak hardness is found at 65 HV at 8 hours of aging and was calculated by deriving the expressed function to a second order polynomial and then solving for it. The spread of dots are the hardness measurements during different time of aging.

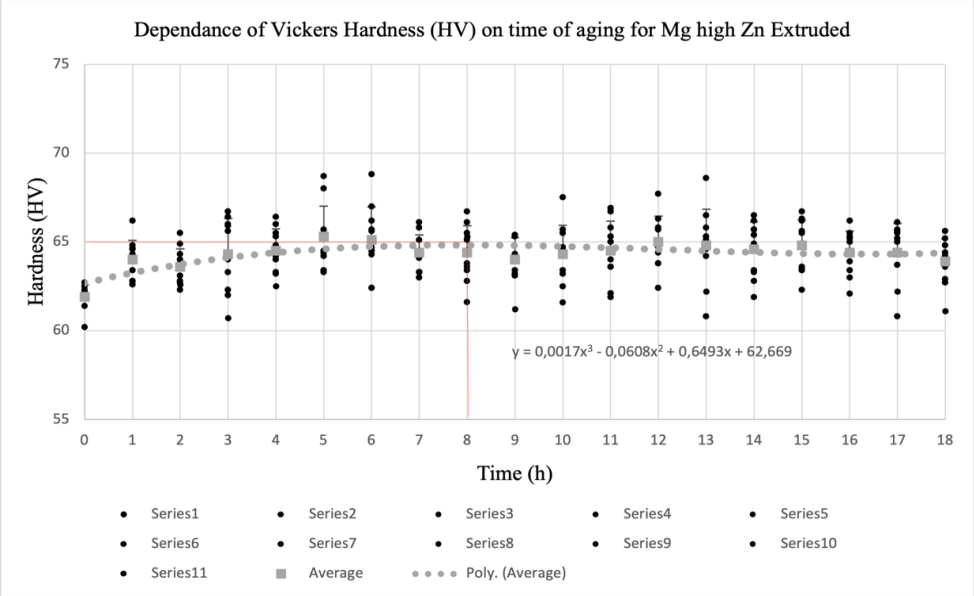

Figure 25: Diagram showing the dependence of Vickers Hardness (HV) on time for Mg high Zn alloy in extruded condition. Dots indicate experimental measurements, while dashed line show polynomial fitting. Peak aging is indicated with red line.

The surface morphology and indentation imprints at different aging hours are presented in figure 26. The initial hardness before the aging took place resulted in 66.1 HV. There are some noticeable darker spots at the surface and a deformed surface with no visible twins, see figure 26a). Moreover, figure 26b) shows the indentation and surface at 7 hours of aging

which resulted in a hardness of 67.7 HV. The parallel grinding or polishing direction is visible in figure 26b) since scratches are obvious. Found in figure 26c) is one of the idents from the peak aging stage at 13 hours and a hardness of 69.6 HV. However, grain boundaries with different sizes along with a scratch around the indentation, also found in figure 26). Presented in figure 26d) are more grain boundaries with different sizes but also some darker spots distributed throughout the surface. Figure 26d) is the overaged stage with a hardness of 67.3 HV after 18 hours.

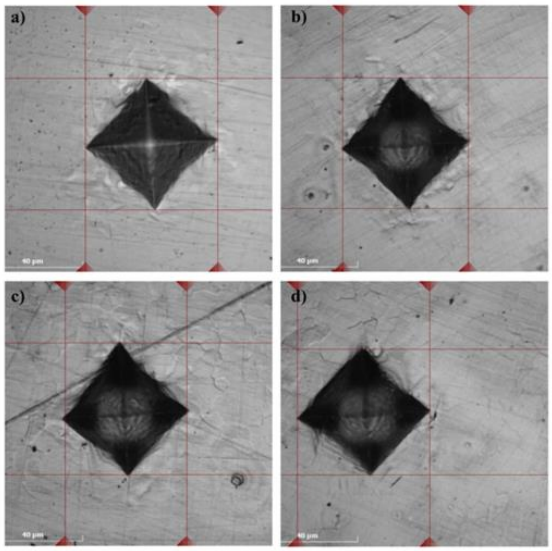

Figure 26: Indentations at different aging times. A) 0 hours, b) 7 hours, c) 13 hours and d) 18 hours.

Figure 27 shows the peak aging for the magnesium medium zinc extruded specimen. The plotted graph is a dashed line of third polynomial order with an expressed function found in figure 27 that best fits the collected data from the hardness test. The peak hardness is found at 69.6 HV at 14 hours of aging and was calculated by deriving the expressed function to a second order polynomial and then solving for it. The spread of dots are the hardness measurements during different time of aging.

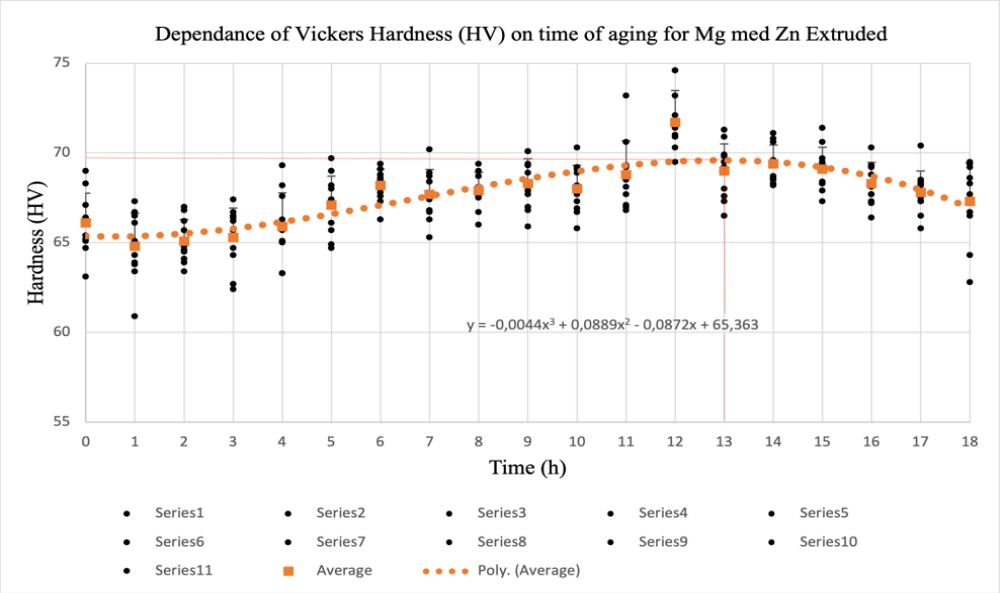

Figure 27: Diagram showing the dependence of Vickers Hardness (HV) on time for Mg medium Zn alloy in extruded condition. Dots indicate experimental measurements, while dashed line show polynomial fitting. Peak aging is indicated with red line.

The indentation imprints at different hours during the aging heat treatment for the magnesium low zinc extruded is visualized in figure 28. The indentation at 0 hours resulted in a hardness of 65.4 HV, before the specimen was put in the silicon oil bath is presented in figure 28a), the surface shows numerous of darker spots that possibly could be corrosion, impurities or precipitates. Figure 28b) is an indentation taken from at 7 hours of aging which resulted in a hardness of 70.7 HV. Scratches The surface has multiple scratches in different direction which comes from the polishing and no deformation around the indentation is evident, see figure 28b). Furthermore, figure 28c) is at peak aging which resulted in a hardness of 72.5 HV in 14 hours of aging. Deformation pattern around the indentation and grain boundaries are visible in figure 28c). Over aging at 18 hours with a hardness of 69.7 HV and a surface with dark regions are found in figure 28d). Silicon oil particles, damaged surface of what looks to be corrosion and scratches are also discovered in figure 28d).

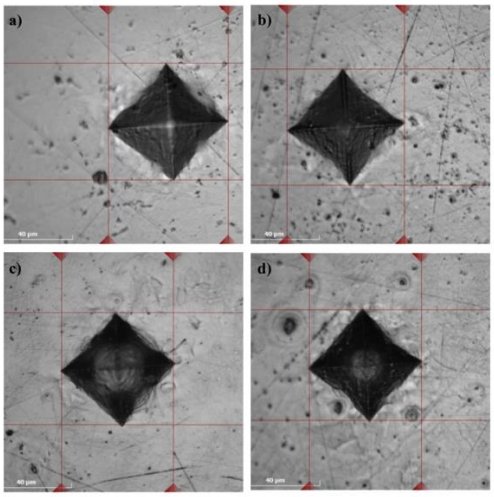

Figure 28: Indentations at different aging times. A) 0 hours, b) 7 hours, c) 14 hours and d) 18 hours.

Figure 29 shows the peak aging for the magnesium low zinc extruded specimen. The plotted graph is a dashed line of third polynomial order with an expressed function found in figure 29 that best fits the collected data from the hardness test. The peak hardness is found at 72.5 HV at 14 hours of aging and was calculated by deriving the expressed function to a second order polynomial and then solving for it. The spread of dots are the hardness measurements during different time of aging.

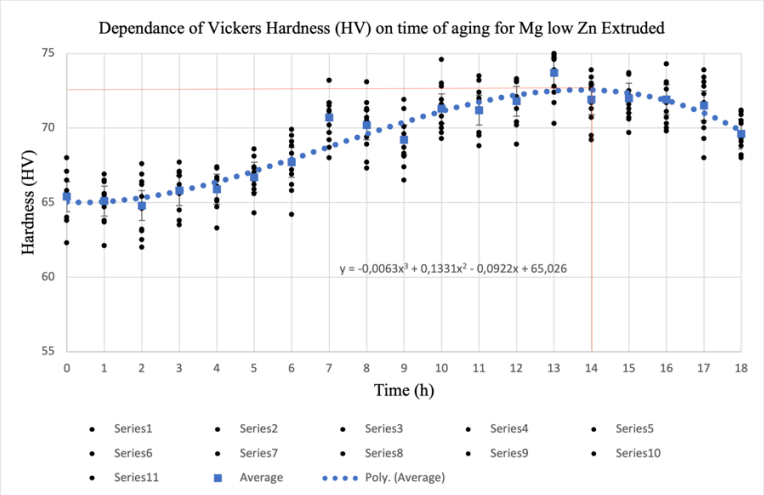

Figure 29: Diagram showing the dependence of Vickers Hardness (HV) on time for Mg low Zn alloy in extruded condition. Dots indicate experimental measurements, while dashed line show polynomial fitting. Peak aging is indicated with red line.

Shown in figure 30 are the summarized hardness measurements for the homogenized specimens at different zinc alloying composition and their peak aging hour. The Mg low Zn had an initial hardness of 63.8 and a peak hardness of 68.6 HV after 18 hours. Additionally, Mg medium Zn started off with an initial hardness of 53.5 HV and reached peak aging also at 18 hours with a maximum hardness of 70 HV, see figure 30. Nonetheless, the hardest homogenized Mg-Zn alloy was the one with highest concentration of zinc, see figure 30. The

initial hardness before aging was 61.6 HV with the peak aging after 17 hours that resulted in a 74 HV.

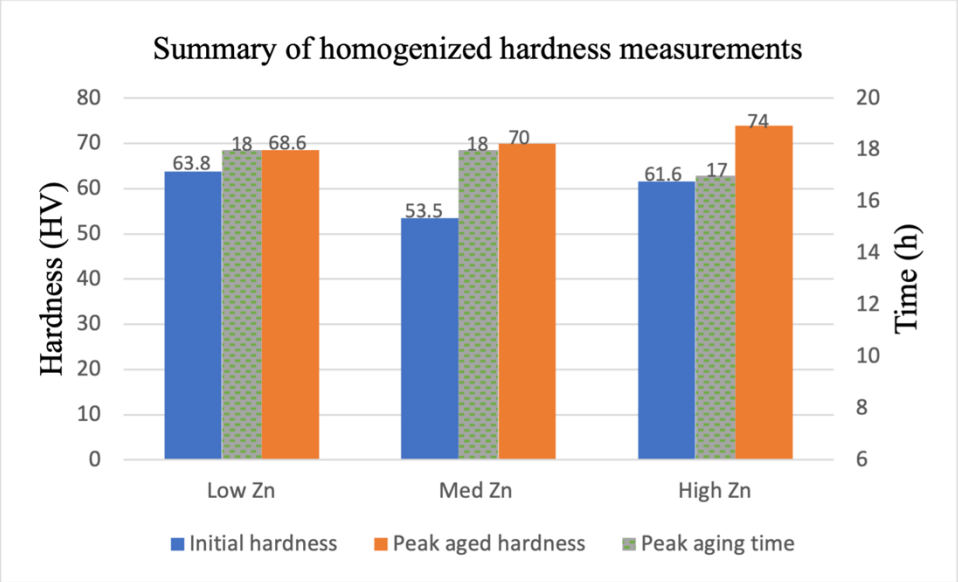

Figure 30: Summary of homogenized hardness measurements.

The summarized hardness measurements of the extruded specimen at different zinc alloying composition are found in figure 31. The Mg low Zn had an initial hardness was 65.4 HV before aging while the hardness peak aging was 72.5 HV after 14 hours, which was the hardest of the extruded Mg-Zn alloys, see figure 31. Moreover, Mg medium Zn had an initial hardness of 66.1 HV before aging heat treatment and resulted in a hardness of 69.6 HV at peak aging after 13 hours. Furthermore, the initial hardness for Mg high Zn was 61.9 HV and the hardness at its peak after 8 hours was 65 HV.

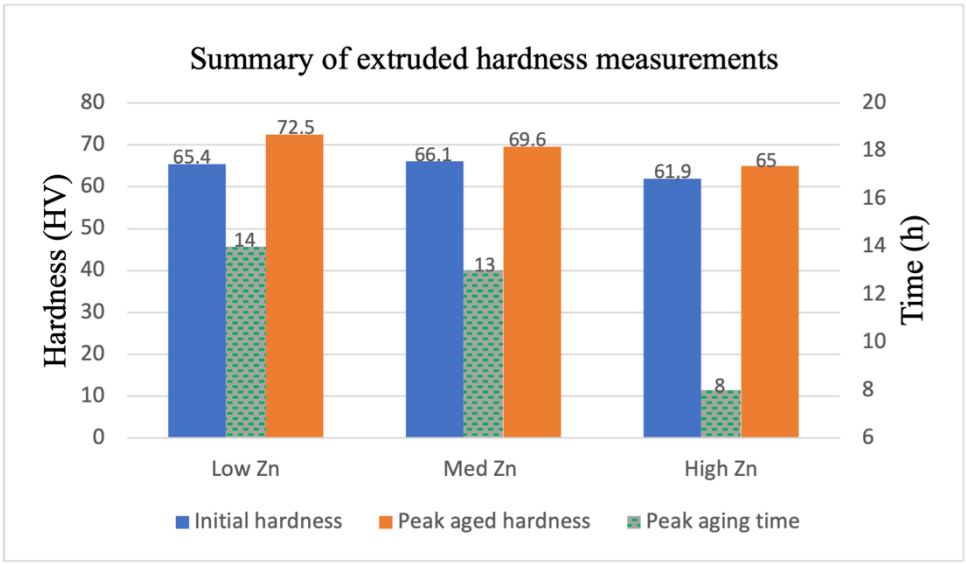

Figure 31: Summary of extruded hardness measurements.

4.2. Microstructure characterization

The SEM result are split in two parts, the surface morphology and EDS.

4.2.1 Surface morphology

Figure 32a) shows the surface of the Mg medium Zn homogenized specimen at the magnification of 100x, marked in red circles are areas where bright particles are prominent. Figure 32a) also shows large grains with similar grain sizes. Figure 32b) delves deeper into the layers of the specimen with magnification of 200x. The results show surface morphology of grains, bright particles circled in red while elongated morphology is squared in red. Furthermore, a contrast between bright and darker regions is also noticeable. Additionally, the results from figure 32c) with BSE at 500x magnification still show bright particles, the darker elongated morphology inside the grain boundaries are also more visible and has been marked with squares in red. The result from BSE 1000x in figure 32d) still show bright particles and the darker elongated morphology inside grain boundaries. The results at 1000x also show other particles with different shapes and sizes, see figure 32d).

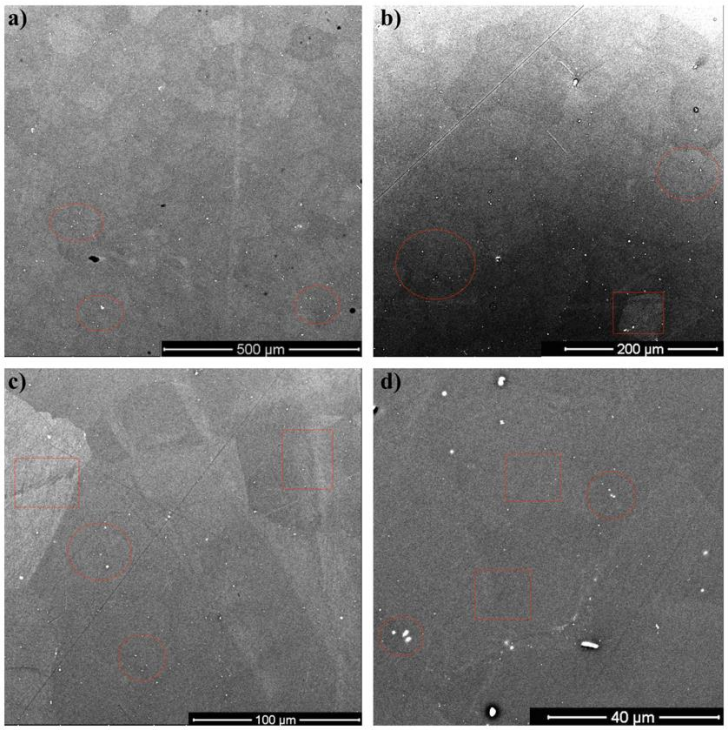

Figure 32: SEM images of Mg medium Zn homogenized. A) BSE-100x, b) BSE-200x, c) BSE-500x, d) BSE 1000x.

The results from the overaged Mg medium Zn homogenized specimen results in multiple visible grain boundaries with different shapes and sized in figure 33a) at 100x magnification. The bright particles in figure 33a) are also visible in figure 33b) at 500x magnification. These bright particles tend to be more presentative around the grain boundary. The result from the 500x magnification is deeper into the specimen surface hardly show no visible scratches, see figure 33b).The grain illustrated from the result in figure 33c) at 1000x magnification is at the crossroad of grain boundaries where other grain with different pattern and size meet, however numerous bright particles also present, see figure 33c). Multiple black elongated morphology and at larger size are visible inside the grains shown in figure 33c). At 5000x magnification presented in figure 33d) further shows the grain boundaries where multiple grains meets. The

results from figure 33d) show that the bright particles tend to be more apparent and larger around the grain boundary.

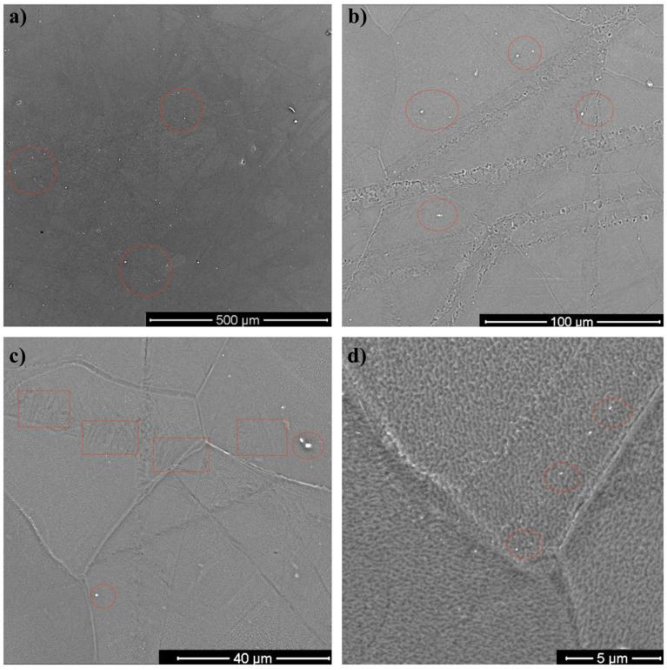

Figure 33: SEM images of MG medium Zn homogenized over aged. A) BSE-100x, b) BSE-500x, c) BSE-1000x, d) BSE 5000x.

The results from the Mg high Zn extruded found in figure 34a) show a variety of bright particles distributed thought the surface. The results from 100x magnification also show clusters of bright particles distributed throughout the surface, circled in yellow, see figure 34a). Moreover, there are noticeable grains of different sizes illustrated in figure 34b) at 500x magnification along with obvious bright particles. These grains are more evident in figure 34c) with 1000x magnification but the bright particles are more clearly shown along with some long dark elongated morphology squared in red, see figure 34c). The appearance of these elongated morphology is more recognizable in figure 34d). Different grain size, white spots, scratches and a regional contrast can also be noted from the result of magnification at 5000x in figure 34d).

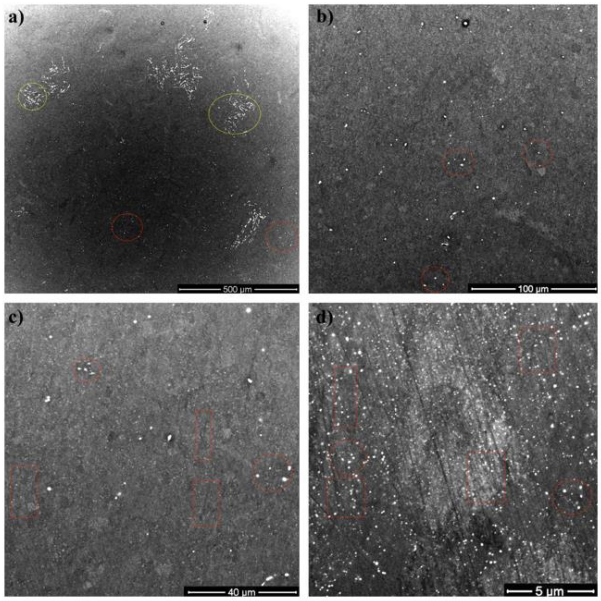

Figure 34: SEM images of Mg high Zn extruded. A) BSE-100x, b) BSE 500x, c) BSE-100x, d) BSE-500x.

SEM results from the overaged specimen of Mg high Zn extruded is visualized in figure 35. From 100x magnification in figure 35a), there are clear clusters of bright particles, these are circled in yellow in figure 35a). Also, more bright particles spread around the surface which are marked in red are present in figure 35a). Deeper into the surface at 500x magnification show more bright particles, these are more obvious around grain boundaries, a cluster of bright particles with different shapes circled in yellow and sizes are also noticeable, see figure 35b). The results from the 1000x magnification in figure 35c) shows multiple grain boundaries with similar grain sizes. Apart from the bright particles, multiple thin but long elongated morphology, marked in red squares can be detected inside the grain boundaries. Figure 35d) at 5000x magnification presents multiple grain boundaries of different sizes. In addition, there are apparent bright particles and darker elongated morphology distributed throughout the specimen surface, particularly around the grain boundaries, see figure 35d).

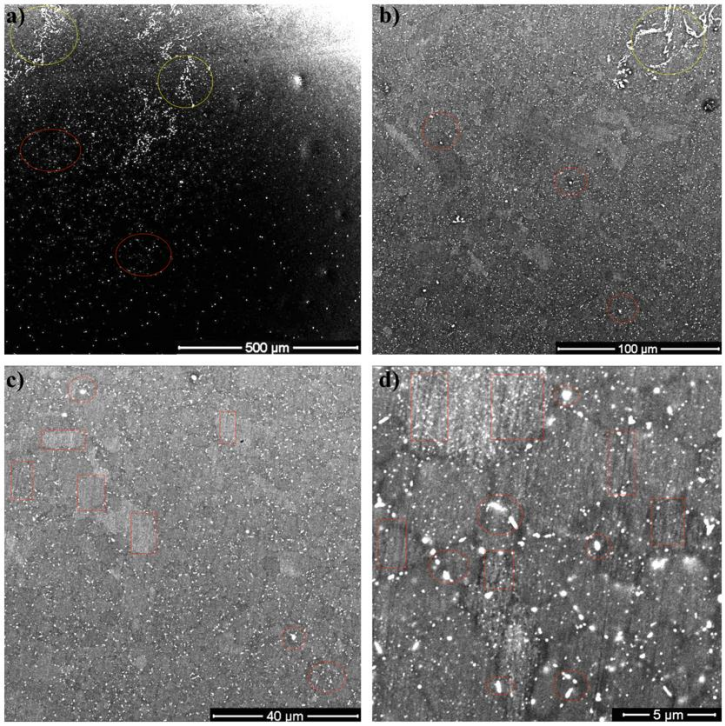

Figure 35: SEM images of Mg high Zn extruded overaged. A) BSE-100x, b) BSE-500x, c) BSE-1000x, d) BSE-5000x.

Mg low Zn extruded BSE result with different magnifications from SEM are found in figure 35. There are obvious scratches from the grinding and polishing stage which are found in figure 36a) but there are also small bright particles marked in red which can be noted in figure 36a). The results also show a cluster of bright particles marked in yellow, presented in figure 36a). Deeper into the specimen surface at 500x magnification shows a distinct contrast between brighter and darker regions and the bright particles are more noticeable while grain boundaries also are visible, see figure 36b). The specimen surface magnified 1000x provides more noticeable grain boundaries where their sizes can be compared as illustrated in figure 36c). Furthermore, there are some darker visible elongated morphologies that can be found in figure 36c). Results from 5000x magnification in figure 36d) presents multiple bright particles but there are also elongated morphology spread throughout the specimen surface in figure 36d). The bright particles seem to be more present around the grains while the elongated morphology are more present inside the grains.

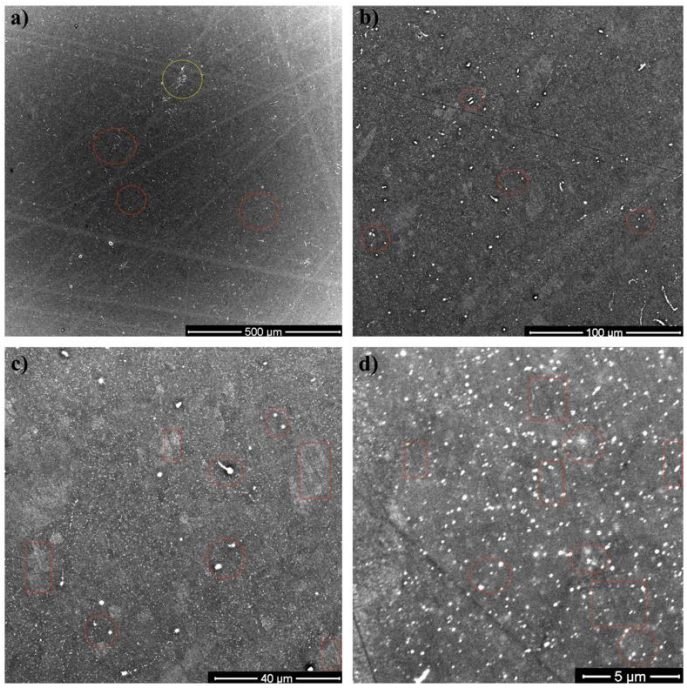

Figure 36: SEM images of Mg low Zn extruded. A) BSE-100x, b) BSE-500x, c) BSE-1000x, d) BSE-5000x.

Figure 37 is from extruded Mg low Zn in the overaged stage. From figure 37a) there are visible grain boundaries, difference it contrasts between brighter and darker regions in the surface along with bright particles and thin dark elongated morphology found at different locations spread throughout the surface. Furthermore, darker elongated morphology can be noted in figure 37b) but also a scratch that goes through a cluster of a large white particle with a different size compared to the other bright particles that usually are circles. The result found in figure 37c) is at a different location in the surface immediately after the specimen had gone through the ion polishing etching machine.With 800x magnification displayed in figure 37c) grain boundaries of different sizes and shapes are evident along with bright particles of circular form. Figure 37d) taken from 3000x magnification further delves deeper into the surface, the patterns and structure of the grains are obvious while the bright particles inside the grain boundaries are visibly clear.

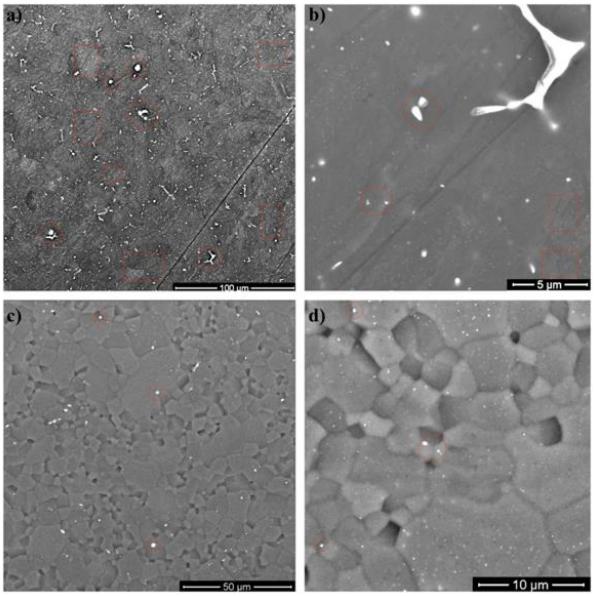

Figure 37: SEM images of Mg low Zn extruded overaged. A) BSE-500x, b) BSE-5000x, c) BSE-800x, d) BSE-3000x.

4.2.2 EDS analysis

Different spots on the specimen surface were taken with EDS analysis. The spots have been categorized as different spot types. Spot type 1 in red are the bright particles, spot type 2 in yellow is the matrix regions and spot type 3 in green are dark elongated morphology, see figure 38. The EDS diagram and table composition for one of the spots in spot type 1, 2 and 3 is found in Appendix 1.

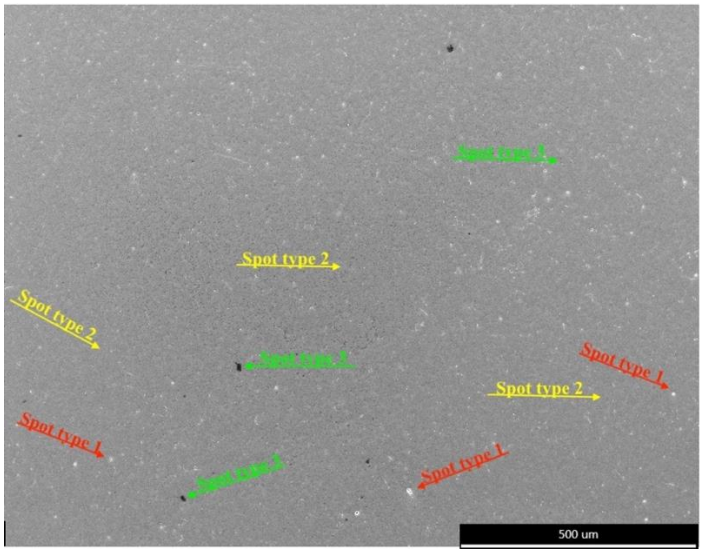

Figure 38: EDS analysis of studied spots for Mg low Zn extruded.

Listed in table 2 are the identified elements obtained from every spot with EDS analysis for Mg low Zn extruded. The results from table 2 regarding the atomic % composition at the different spot types is calculated by adding the atomic % of the spots within a spot type and then finding the average.

Table 2: Chemical composition (in atomic %) of a material in various spots identified in Figure 38 from EDS analysis in Mg low Zn extruded specimen.

	Spot type		
Identified elements	1 – Bright particles	2 – Matrix	3 – Elongated morphology
Mg	97.85	98	97
Zr	0	0	0
Ca	0	0	0
Fe	0	0	0
Ni	0	0	0
Cu	0	0	0
Zn	3.2	1.2	1.19
O	0	0	3.3
Na	0	0	2.19
Ar	0	0	0

Listed in table 3 are the identified elements obtained from every spot with EDS analysis for Mg medium Zn homogenized. The results from table 3 regarding the atomic % composition at the different spot types is calculated by adding the atomic % of the spots within a spot type and then finding the average.

Table 3: Chemical composition (in atomic %) of a material in various spots identified in Figure 38 from EDS analysis in Mg medium Zn homogenized specimen.

	Spot type		
Identified elements	1 – Bright particles	2 – Matrix	3 – Elongated morphology
Mg	73	98.5	80.1
Zr	15	0.003	0.04
Ca	0.3	0.14	5.61
Fe	0.5	0.09	0.08
Ni	0.22	0.07	0.06
Cu	0.19	0.06	0.05
Zn	10.5	1.05	0.74
O	0	0	19.9
Na	0	0	0
Ar	0	0	0

Listed in table 4 are the identified elements obtained from every spot with EDS analysis for overaged Mg medium Zn homogenized. The results from table 4 regarding the atomic % composition at the different spot types is calculated by adding the atomic % of the spots within a spot type and then finding the average.

Table 4: Chemical composition (in atomic %) of a material in various spots identified in Figure 38 from EDS analysis in overaged Mg medium Zn homogenized specimen.

	Spot type		
Identified elements	1 – Bright particles	2 – Matrix	3 – Elongated morphology
Mg	49	98.6	98.64
Zr	0.07	0.05	0.1
Ca	5.7	0.1	0.12
Fe	5.7	0.08	0.09
Ni	4.4	0.07	0.07
Cu	0.04	0.05	0.05
Zn	0.4	1	0.92
O	51	0	0
Na	0	0	0
Ar	1.13	0	0

The summarized chemical composition results of the bright particles, spot type 1 for Mg medium Zn homogenized, overaged Mg medium Zn and Mg low Zn extruded is found in table 5.

Table 5: Summarized chemical composition (in atomic %) of spot type 1 for the different zinc concentration and processing of Mg alloys.

	Spot type – 1		
Identified elements	Med Zn homo	Overaged Med Zn homo	Low Zn extruded
Mg	73	49	97.85
Zr	15	0.07	0
Ca	0.3	5.7	0
Fe	0.5	5.7	0
Ni	0.22	4.4	0
Cu	0.19	0.04	0
Zn	10.5	0.4	3.2
O	0	51	0
Na	0	0	0
Ar	0	1.13	0

The summarized chemical composition results of the matrix, spot type 2 for Mg medium Zn homogenized, overaged Mg medium Zn and Mg low Zn extruded is found in table 6.

Table 6: Summarized chemical composition (in atomic %) of spot type 2 for the different zinc concentration and processing of Mg alloys.

	Spot type 2		
Identified elements	Med Zn homo	Overaged Med Zn homo	Low Zn extr
Mg	98.5	98,6	98
Zr	0.05	0.05	0
Ca	0.14	0.1	0
Fe	0.09	0.08	0
Ni	0.07	0.07	0
Cu	0.06	0.05	0
Zn	1.05	1	1.2
O	0	0	0
Na	0	0	0.3
Ar	0	0	0

The summarized chemical Icomposition results of the elongated morphology, spot type 3 for Mg medium Zn homogenized, overaged Mg medium Zn and Mg low Zn extruded is found in table 7.

Table 7: Summarized atomic % for the identified elements for spot type 3, the dark elongated morphology for the different zinc concentration and processing of Mg alloys.

Identified elements	Med Zn homo	Overaged Med Zn homo	Low Zn extr
Mg	80	98,6	97
Zr	0.05	0.05	0
Ca	0.14	0.1	0
Fe	0.09	0.08	0
Ni	0.07	0.07	0
Cu	0.06	0.05	0
Zn	1.05	1	1.2
O	19.9	0	3.33
Na	0	0	2.19
Ar	0	0	0

4.3. Grain size analysis

Figure 39 shows horizontal lines that intersect grain boundaries to calculate the mean intercept length for the Mg medium Zn homogenized surface.

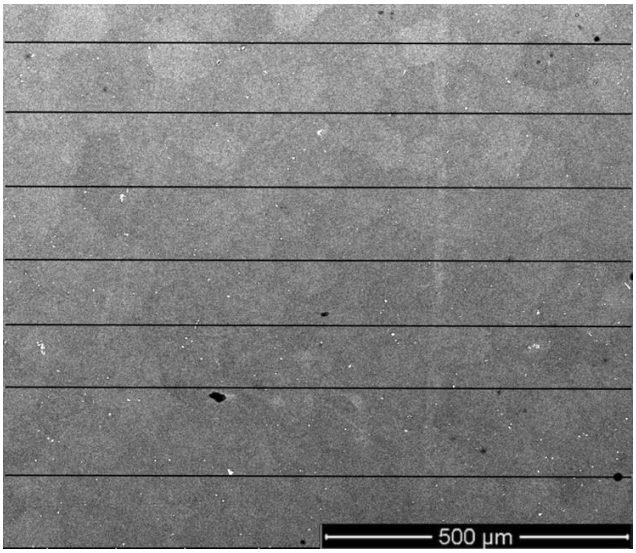

Figure 39: Mg medium Zn homogenized line interception of grains.

Figure 40 summarizes the quantitative analysis of boundary intercepts for the Mg medium homogenized specimen. Total of 7 horizontal lines were drawn with an equal length of 1490 µm, which was the width of the obtained image captured by SEM. This resulted in a mean intercept length of 39 µm. The calculations were made by using equation 2 and 3.

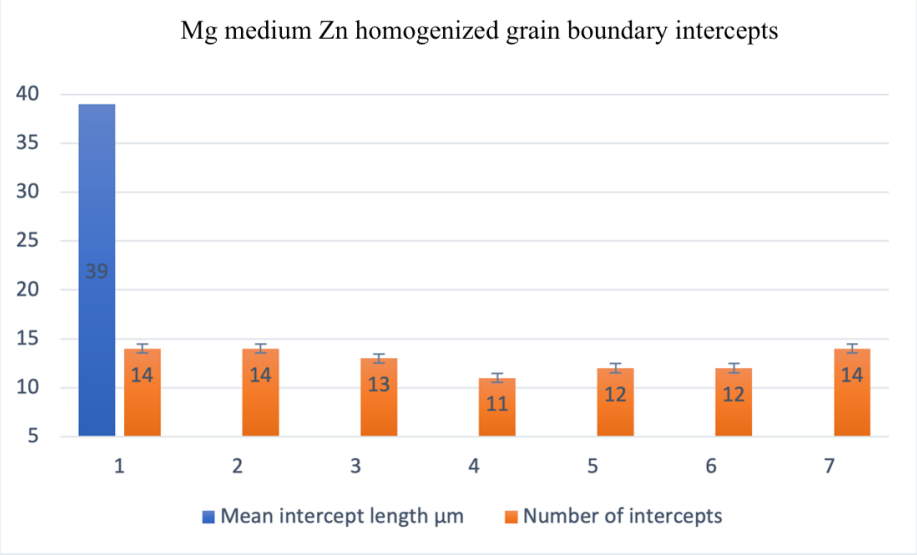

Figure 40: Mg medium Zn homogenized grain boundary intercepts.

Figure 41 shows horizontal lines that intersect grain boundaries to calculate the mean intercept length for the overaged Mg medium Zn homogenized surface.

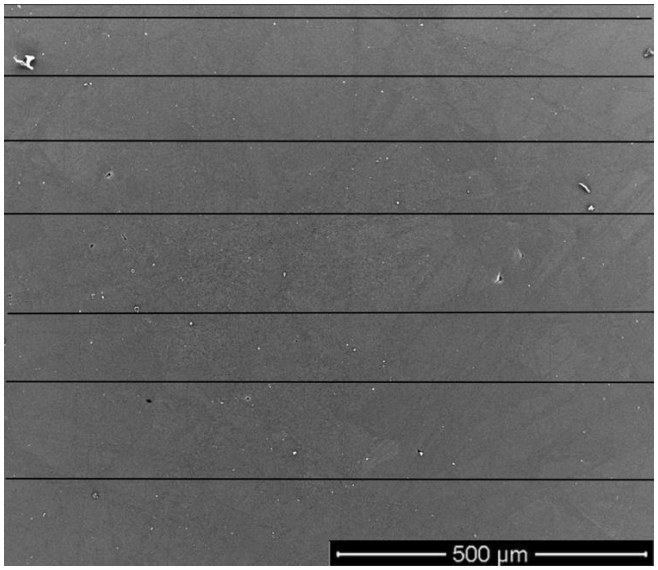

Figure 41: Overaged Mg medium Zn homogenized line interception of grains.

Figure 42 summarizes the quantitative analysis of boundary intercepts for the overaged Mg medium homogenized specimen. Total of 7 horizontal lines were drawn with an equal length of 1490 µm, which was the width of the obtained image captured by SEM. This resulted in a mean intercept length of 31µm. The calculations were made by using equation 2 and 3.

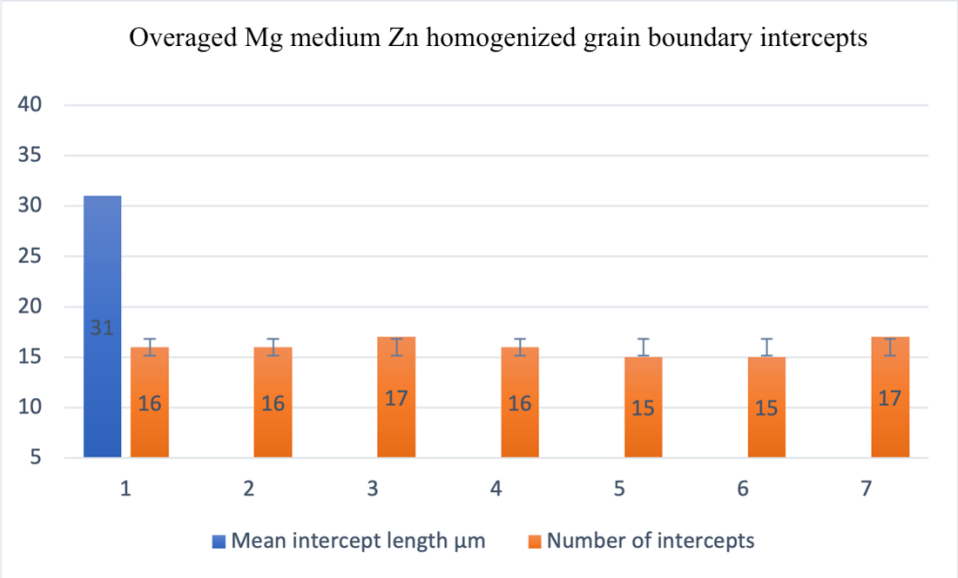

Figure 42: Overaged Mg medium Zn homogenized grain boundary intercepts.

Figure 43 shows horizontal lines that intersect grain boundaries to calculate the mean intercept length for the Mg high Zn extruded surface.

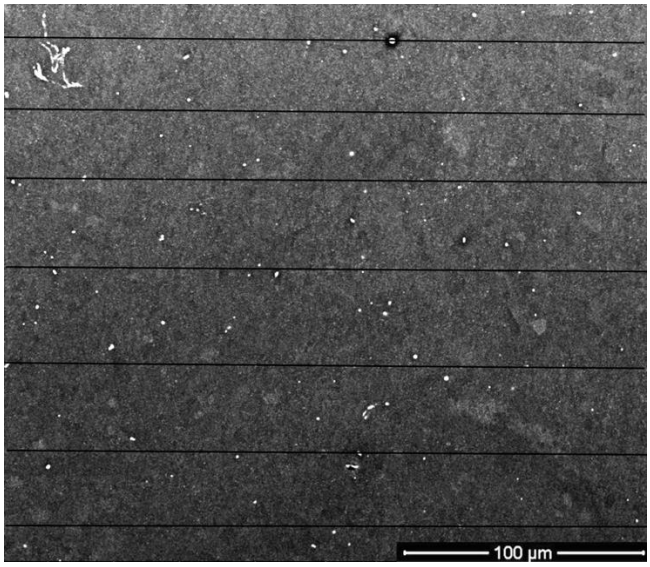

Figure 43: Mg high Zn extruded line interception of grains.

Figure 44 summarizes the quantitative analysis of boundary intercepts for the Mg high Zn extruded specimen. Total of 7 horizontal lines were drawn with an equal length 298 µm, which was the width of the obtained image captured by SEM. This resulted in a mean intercept length of 6.1 µm. The calculations were made by using equation 2 and 3.

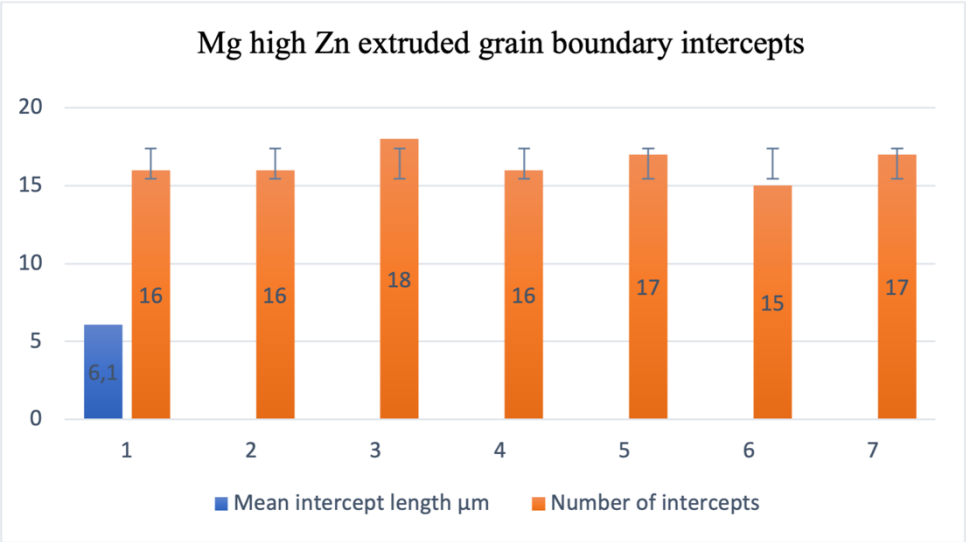

Figure 44: Mg high Zn extruded grain boundary intercepts.

Figure 45 shows horizontal lines that intersect grain boundaries to calculate the mean intercept length for the overaged Mg high Zn extruded surface.

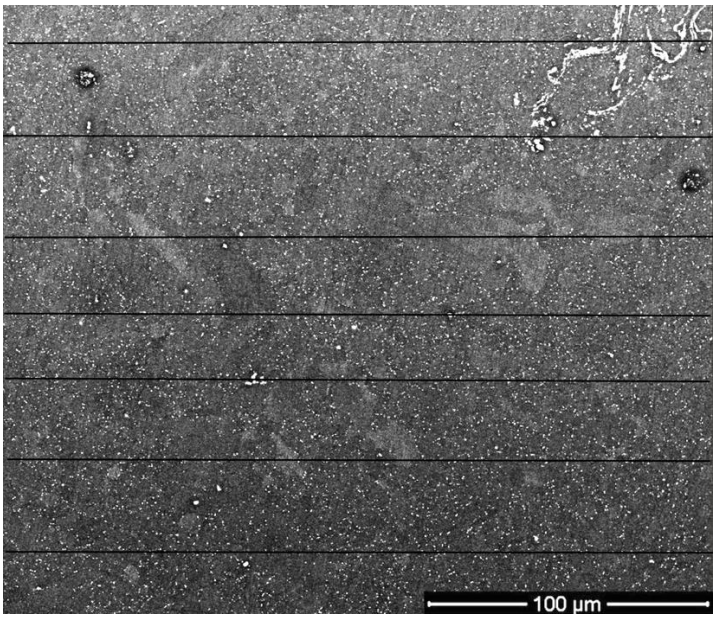

Figure 45: Overaged Mg high Zn extruded line interception of grains.

Figure 46 summarizes the quantitative analysis of boundary intercepts for the overaged Mg high Zn extruded specimen. Total of 7 horizontal lines were drawn with an equal length 298 µm, which was the width of the obtained image captured by SEM. This resulted in a mean intercept length of 5.6 µm. The calculations were made by using equation 2 and 3.

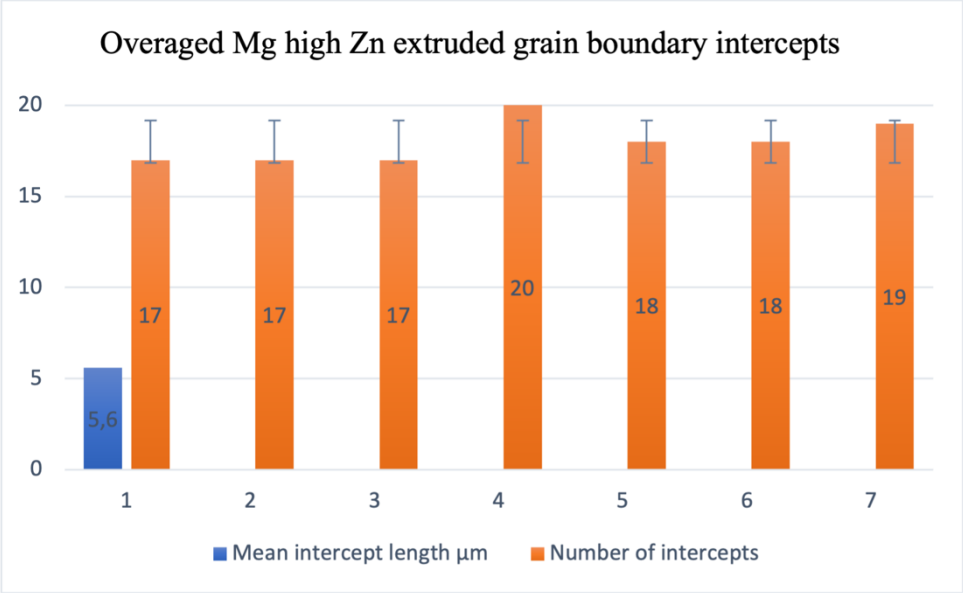

Figure 46: Overaged Mg high Zn extruded grain boundary intercepts.

Figure 47 shows horizontal lines that intersect grain boundaries to calculate the mean intercept length for the Mg low Zn extruded surface.

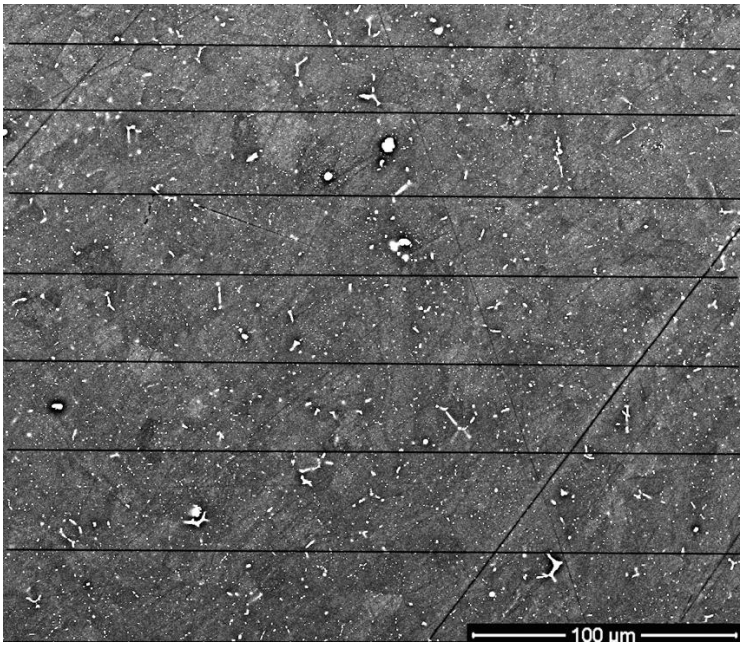

Figure 47: Mg low Zn extruded line interception of grains.

Figure 48 summarizes the quantitative analysis of boundary intercepts for the Mg low Zn extruded specimen. Total of 7 horizontal lines were drawn with an equal length 298 µm, which was the width of the obtained image captured by SEM. This resulted in a mean intercept length of 6 µm. The calculations were made by using equation 2 and 3.

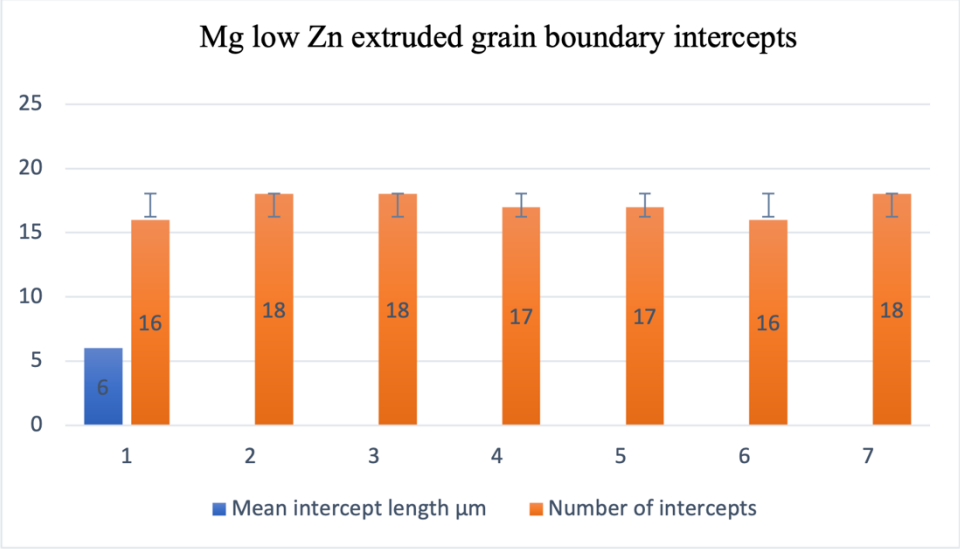

Figure 48: Mg low Zn extruded grain boundary intercepts.

Figure 49 shows horizontal lines that intersect grain boundaries to calculate the mean intercept length for the overaged Mg low Zn extruded surface.

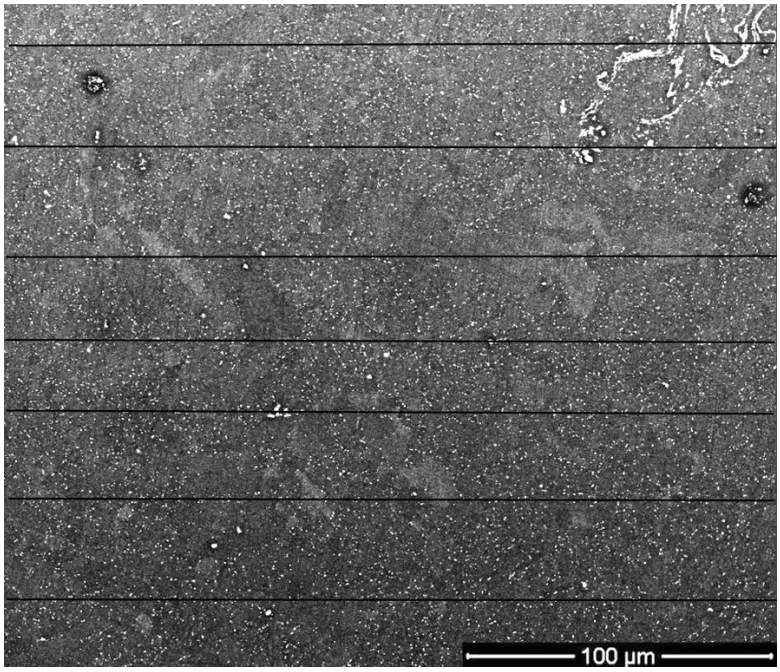

Figure 49: Overaged Mg low Zn extruded line interception of grains.

Figure 50 summarizes the quantitative analysis of boundary intercepts for the overaged Mg low Zn extruded specimen. Total of 7 horizontal lines were drawn with an equal length 298 µm, which was the width of the obtained image captured by SEM. This resulted in a mean intercept length of 5.4 µm. The calculations were made by using equation 2 and 3.

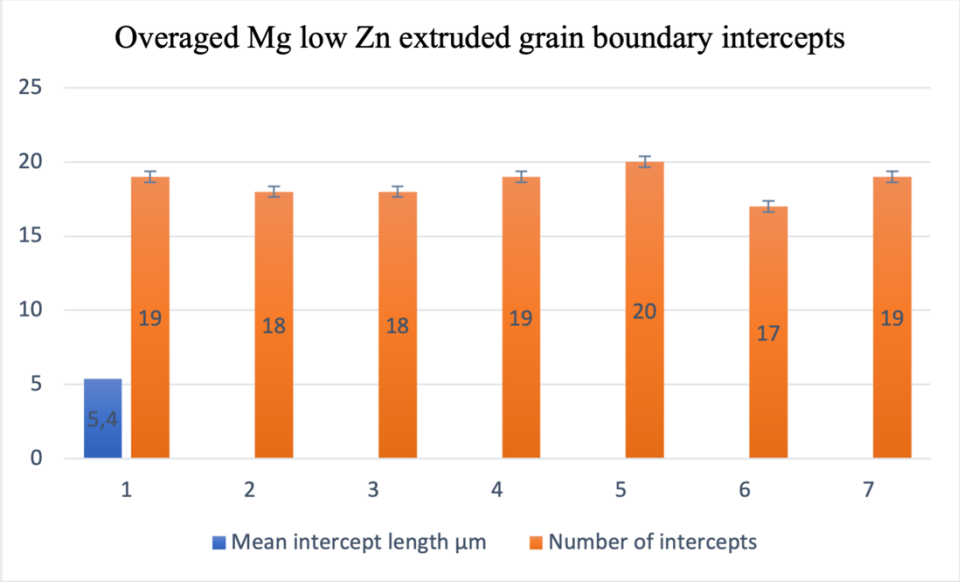

Figure 50: Overaged Mg low Zn extruded grain boundary intercepts.

5. Analysis and discussion

5.1. Hardness evolution and peak aging

Based on the results presented in subsection 4.1, the quantity of zinc and the processing of Mg alloys have a significant impact on maximum strength acheved in this material, as represented by Vickers hardness (HV) in this study, and its kinetics.

The indentations taken at different aging times from the homogenized specimens, figures 18, 20 and 22, along with the similar measurements on the extruded specimens, figures 24, 26 and 28, show heterogeneity characteristic the specimens mechanical behavior changes depending on direction once it has deformed, this phenomenon leads to increase in hardness owing to the Mg-Zn alloys being HCP crystal which is thoroughly explained by (Smallman et al., 1999). Twinning which is a microstructural parameter plays an integral part in hardening of a material. However, twins are limited in room temperature considering the scare number of slip and twinning systems activated with basal slip being the predominant slip system. The most common twin boundaries in magnesium are the $\{10\bar{1}2\}$ slip plane in the $< 1011 >$ slip direction, particularly below 225 °C which is stated by the publication by (Kaya et al., 2005). This statement aligns with the findings of the twins before aging in figure 18a) and with the other twins found in figure 20 and figure 22 due to the constant aging temperature of 180 °C.

The initial hardness results before aging for the homogenized material were 63.8 HV for low Zn, 53.5 HV for medium Zn and 61.6 HV for high Zn found in figure 19, 21, 23 and summarized in figure 30. This is unpredictable since its contradictory to the standard norm which is that the contribution of Zn to the Mg will lead to increased hardness, this is emphasized in the study from (Somekawa et al., 2006). However, the hardness results at peak aging for the homogenized specimens at 68.6 HV for low Zn, 70 HV for medium Zn and 74 HV for high Zn are consistent to the reasoning in the report from (Clark, 1965). The report written by (Clark, 1965) shed lights on how the kinetics of Zn has a direct impact in the aging process, this remark is parallel with the results considering that the specimen with the highest Zn concentration eventually turned out to be the hardest at 74 HV for the high Zn homogenized specimen. The reason behind this is due to the precipitation kinetics at higher Zn concertation that influences the aging condition. The added zinc atoms diffuse to multiple nucleate that lead to growth of principates which hinders dislocation thereby hardens the material, this is extensively detailed in the document by (Askeland et al., 2010) and in section 2.5.

The hardness measurement from the extruded specimens before aging were 65.4 HV for low Zn, 66.1 HV for medium Zn and 61.9 HV for high Zn, these are found in figure 25, 27, 29 and summarized in figure 31. The hardness measurement results before aging for the extruded specimen were higher than the homogenized in their respective Zn concentration. These results are consistent with expectations due to extrusion affects the microstructural parameters such as grain size, texture and twins and therefore increases the hardness during the extrusion process as described by (Zeng et al., 2019). However, the peak hardness results for the extruded specimens at peak aging were 72.5 HV for low Zn, 69.6 HV for medium Zn and 65 HV for high Zn. These results contradict statements by (Clark, 1965) that alludes to that zinc kinetics directly impacts the aging process due to precipitation and therefore makes the material harder. Mindful that the extruded low Zn resulted in highest peak aged hardness out of the other extruded specimens namely, medium Zn and high Zn, found in figure 31 matches the discussion brought up by (Xu et al., 2012). The discussion by (Xu et al., 2012)

accentuate how extrusion makes a material undergoe plastic deformation and changes in recrystallization of texture and dynamic precipitation, this improves the stretching mechanics and make dislocation motion more difficult, therefore hardens the material. Although the extrusion impacts the material hardness, it seems to also affect the zinc kinetics of the Mg-Zn alloy. The kinetics of zinc atoms seem to have been diffused during the extrusion process and exert influence on strengthening the material, which seems to be the case since extruded low and extruded medium zinc had an initial hardness of 66.1 HV and 65.4 HV respectively compared to 61.9 HV for high zinc. The experimental observations from the results in figure 31 correlates with the present discussion. However, multiple experimental tests should be done to confirm this statement.

It should be stressed that the main difference between the homogenized and extruded results is the processing of Mg alloys that affects the microstructure, consequently impacting the hardness. At room temperature, extruded Mg-Zn is harder due to finer grain structure and higher dislocation density, this is underlined in the publication by (Tong et al., 2013). During aging, the homogenized Mg-Zn alloys achieves the higher hardness because of more coherent precipitates that effectively impede dislocation movement, the precipitates grow larger and becomes more spaced during aging, leading to increase in hardness. This is underlined in the experiments by (Cha et al., 2022) and supports the arguments for the contrast in hardness when comparing the results of homogenized and extruded values in figure 30 and figure 31.

Additionally, the hardness values increased significantly more in the homogenized Mg-Zn alloys compared to the extruded Mg-Zn values, particularly for the homogenized Mg medium Zn alloy in figure 21that starts with a hardness of 53.5 HV and peaks at 70 HV in contrast to extruded Mg medium Zn alloy in figure 27 that starts with a hardness of 66.1 and peaks at 69.6 HV or the extruded high Zn that starts from 61.9 HV and peaks at 65 HV. This is because of the different grain structure after processing of Mg alloys which leads to a completely different precipitation formation and density during the aging, similar explanation is given by (Callister et al., 2018, ASM, 1991).

Another variable that needs to be pinpointed is the zinc concentration which affects the peak aging kinetics. The reason behind this is based on the premise of the slopes of the curves for high Zn homogenized in figure 19 and high Zn extruded in figure 25, although the zinc atoms may have been diffused during the extrusion process which led to several nucleation forming, subsequently growth of precipitates. With the result of homogenized Mg-Zn alloys borne in mind, peak aging is reached faster with higher zinc concertation. This phenomenon can be seen from the viewpoint of Ficks law of diffusion, the age hardening of Mg-Zn alloys lies in diffusion of zinc atoms during the heat treatment process which influences the mechanical properties of the alloy such as precipitates. The more zinc concentration there is, the faster kinetic diffusion, considering that the Mg-Zn age hardening process involves diffusion of zinc atoms in the magnesium material. This diffusion process follows Ficks law where the diffusion rate depends on the zinc concentration gradient of the zinc atoms, this affects precipitation formation. Due to higher concentration of zinc, it promotes formation of greater volume fraction of precipitates during aging, Ficks law is profoundly described by (Abbaschian et al., 2009, Smallman et al., 1999). Nonetheless, this reasoning corresponds well to why the homogenized hardness values for the Mg-Zn alloys goes from hardest in the highest zinc concertation and the least hard in the lowest zinc concentration. However, Ficks law seem to not affect the extruded process in a similar way, particularly at higher zinc concentration, hence why the slight hardness change in terms of result for extruded medium and high Zn. Nonetheless, further research on this needs to be made to confirm the statement.

The comparison of how different temperature and aging time affect the hardness is discussed by (Clark, 1965). Mg-Zn alloys in the composition range of 3-8 wt.% age hardens around the temperature 70-260 °C, which support the results obtained from this project due to the age hardening was find with the constant temperature of 180 °C in the composition range of 1-6.2 wt.% Zn. The study from (Mima et al., 1971) finds peak aging in 28 hours for Mg-4 wt.% Zn at 185°C with 62.5 HV with a homogenized processing. The result from homogenized medium Zn found its peak aging after 19 hours with 70 HV for 180 °C. This is inconsistent with expectations since lower temperature usually requires longer aging time and then leads to higher hardness, as in the case for (Buha 2008) with Mg–7 wt% Zn peak aged at 116 HV after 1000 hours during a constant temperature of 70 °C. However, the temperature from the experiments were for 180 °C compared to (Mima et al., 1971) temperature of 185 °C, along with the peak hardness from the experiment at 70 HV in contrast to 62.5 HV does not significantly differ. Although the peak aging time does, results obtained are still credible and reasonable. Other studies like the one by (Clark, 1965) finds maximum hardness of 68.6 HV after 16 hours with a temperature of 204 °C for Mg-5 wt.% Zn alloy, while (Chun et al., 1969) finds peak aging after 15 hours for Mg-5.1 wt.% Zn at 240°C with 65 HV. These findings corelates with the homogenized high Zn peaks at 17 hours with 74 HV since the lower temperature requires longer aging time but eventually ends up becoming harder. Moreover, findings from (Wei et al., 1996) reaches peak aging after 20 hours with a hardness of 70 HV for Mg-9 wt.%. Zn at 240°C, the result from the extruded high Zn stresses the dissimilarity since peak aging is found after 8 hours with 65 HV. One could argue that the peak aging time based on results in figure 19, 21, 23 for the homogenized are remarkably longer than the extruded in figure 25, 27 and 29. Considering that the only changed parameter between the homogenized and extruded specimens are the processing of Mg alloys while the other prerequisites remained the same such as temperature and zinc concentration leads to the assumption that aging time and temperature are affected by the processing of Mg alloys. Whether or not the temperature and aging time are heavily influenced by the processing of Mg alloys could be further investigated in future work.

The spread of dots for the homogenized specimens in figure 19, 21and 23 are larger than the spread of dots for the extruded specimens in figure 25, 27 and 29. The results shows that the homogenized specimen has a larger standard deviation compared to the extruded specimen, hence why the larger spread. This suggests that the homogenized hardness values have a more unpredictability and variety compared to the extruded one. As the heat treatment experimenting progresses, the spread of dots seems to be somewhat larger, see figure 19, 21 and 23. This can be explained by the heterogeneity characteristics in the materials due to the indentations induce sliding and migration at grain boundaries. This can alter the grain boundary structure and properties, contributing to the overall heterogeneity as (Humphreys et al., 2004) describes. This suggest that some of the indentations might have hit inside of a grain while other between the grain boundaries and other indentation between triple junction of grains. Therefore, the spread of dots is particularly larger for the homogenized specimens as they also tend to have larger grain size which increases the chances of heterogeneity occurring. (Liu et al., 2024) explains that during the aging process, the material is more prone to different behaviour due to the orientation-dependent formation and distribution of precipitates that influences the crystallographic textures and grain boundaries. These precipitates are affected by the diffusion path on the magnesium matrix. The extruded specimen tends not to have a large diffusion of zinc atoms during aging considering that the low hardness increases from initial hardness to peak aged hardness, see figure 31 compared to figure 30. With regards to that diffusion of zinc and the interaction of precipitates with grain boundaries further enhances anisotropic characterises also explains why the figures 25,

27 and 29 for the extruded specimen not have that large of spared compared to the homogenized ones in figure 19, 21 and 23.This is the reason why the results show large difference hardness values at longer aging time particularly for the homogenized specimen which have been confirmed in the conducted research by (Liu et al., 2022). Since the grain boundaries varies with processing of Mg alloys while also being linked to hardness also explains the large spread of dots that shows the hardness variation, this statement is supported by the analysis by (Liu et al., 2022) highlights the critical role of grain boundaries with the observed differences in hardness between homogenized and extruded states.

The current results regarding aging hardness confirm that the kinetics of precipitation during aging depends primarily on the zinc alloying composition, the mechanical behaviors, the processing of Mg alloys and to a lesser degree the aging temperature. Similar trends were observed in the findings from (Buha et al., 2008) and is consistent findings from (Zhao et al., 2014).

5.2. Surface morphology

When examining the surface morphology of the homogenized Mg-Zn alloy compared to extruded Mg-Zn alloy over aging time using SEM, multiple key observations have been made regarding impurities, texture, grain size, precipitates and surface defects.

There is a distinct difference in the surface when comparing the homogenized specimens before aging in figure 18a), 20a) and 22a) opposed to the extruded specimens before aging figure 24a), figure 26a) and figure 28a), which alludes to the different processing of Mg alloys. Irrespective of the Zn concentration, the surface in figure 18a), 20a) and 22a) for the homogenized specimens show a more uniformed surface with composition segregation and with less darker and brighter spots contrary to the extruded specimens in figure 24a), 26a) and 28a). The surface morphology results when comparing the homogenized and the extruded surface corresponds well with what (Liang et al., 2023) highlights in their study. The results with regards to figure 32a) homogenized Mg medium Zn and figure 33a) homogenized Mg medium Zn overaged show that there are a smaller number of impurities since they are dispursed when homogenized and the surface have a more random texture opposed to figure 34a) extruded Mg high Zn, figure 35a) extruded Mg high Zn overaged, figure 36a) extruded Mg low Zn and figure 37a) extruded Mg low Zn overaged. The reason behind how the surface morphology in the results varies is because of the significant distinction in the processing of the Mg-Zn alloys. The results correspond well with the expectation of how (ASM, 1991) describes a homogenized surface and how (Tong et al., 2013) describes an extruded surface, which also are explained in section 2. 6. The yellow marked circles in figure 34, 35, 36, and 37 in the extruded surface show a cluster of bright particles which is not seen in figure 32 and figure 33 for the homogenized surface owing to that the homogenization process eliminates casting segregation and other particles which is highlighted by (Liu et al., 2018).

When analyzing the results from the BSE in figure 32-37, it indicates that the brighter regions are zinc material while the darker regions are magnesium material owing to zinc having the higher atomic number over magnesium, this is also emphasized in section 2.7. Some grains appears to be brighter and other darker in figure 32-37, this is due to the different grain sizes. However, the red-marked circles and the red squares in figure 32-37 that are referred to bright particles or darker elongated morphology that were exposed under SEM could be various constituents or phases within the alloy. The nature of these particles depends on the parameters such as alloying composition, processing of Mg alloys and the undergone aging

heat treatment. Additionally, the process before heat treatment could also influences the elements being detected by EDS.

Figure 38 illustrates the investigation of certain spots of Mg low Zn extruded with the help of the EDS by categorizing the spots into spot types. The results found in table 2 reveals that spot type 1with the bright particles have identified Mg and Zn as elements, which is no surprise. However, considering that the investigated surface in figure 38 is extruded, one could argue that other elements also possible could be identified, such as calcium (Ca), zirconium (Zr), copper (Cu), iron (Fe), natrium (Na) and nickel (Ni) where trances usually are found in Mg-Zn alloys, as described by (Loukil, 2022). Results in table 2 for the spot type 2 which is the matrix form figure 38 only contained Mg and Zn, which was expected. The dark elongated morphology spot type 3 has been identified with elements such as 1.19 atomic %, oxygen (O) at 3.3 atomic% and natrium at 2.19 atomic %, see table 2. When reflecting that the dark elongated morphology usually is find around the grain boundaries and while also being mindful of the zinc content, this could most likely be specific microstructural features that develops during processing and heat treatment as (Loukil, 2022) explains.

Table 3 for the Mg medium Zn homogenized resulted in more identified elements, which is conflicting with the description of how a homogenized surface thats being underlined in the research by (ASM, 1991). The bright particles resulted in a containing Mg, Zr, and Zn, this is usually the case for zinc-rich phases as they tend to appear as bright particles due to the intermetallic compounds formed between magnesium and zinc, similar explanation is given by (Jiang et al., 2020), these intermetallic compounds are most likely secondary primary precipitates when also considering their coherent shape. Furthermore, the results from the matrix in table 3 is expected although there is a bit of calcium identified. The addition of calcium in the Mg-Zn alloys enhances the mechanical properties and provides corrosion resistance while also forming intermetallic compounds as described by (Roh et al., 2022) which could be the reason its found in every spot type in table 3. The elongated morphology from figure 38 have shown to contain Mg, O, Ca and Zn. Due to the 19.9 atomic % of O when investigating spot type 3, one could make the argument that the reason for the significant emergence of oxygen has to with the specimen being exposed to air. Similar trends can be found when magnesium is exposed to air and quickly develops a thin layer of magnesium oxide due its reaction with oxygen (PubChem, 2024). The content of 0.74 atomic% Zn could be Mg-Zn precipitates which typically appears as plate-like precipitates in the magnesium matrix where they are seen as rod-like, needle-like or plate-like structures outside the boundaries of grains as explained by (Yuan et al., 2021 and Liu et al., 2020). However, these types of secondary precipitates are beyond the resolution used in this study and can therefore not be confirmed.

Table 4 for the overaged Mg medium Zn homogenized resulted multiple identified elements. The purpose of the homogenized surface is to precipitate out different solid phases for them to dissolve in the matrix, but also to eliminate the casting segregation and achieve a uniformed surface as described by (Liang et al, 2023). Following this reasoning the overaged homogenized Mg medium Zn argue against how (Liang et al, 2023) describes a homogenized surface of a specimen when reflecting about the identified elements in table 4. Spot type 1 have more oxygen at 51 atomic% than magnesium at 49 atomic %. A reason behind this is that the specimen is overaged and when magnesium is strongly heated, the oxygen will produce bright white light particles forming magnesium oxide powder, as described by

(PubChem, 2024) and with this reasoning borne in mind, it explains how there is more oxygen than magnesium. The results of matrix in table 4 for spot 2 is predictable with magnesium at 98.6 atomic % and zinc at 1%. However, there is also copper at 0.05 atomic %, the explanation behind this is that copper is a common alloying element in Mg-Zn alloys, the aging can alter the solubility and distribution of copper in the alloy, this is explained by (Loukil 2022). The iron most in spot 2 at 0.08 atomic %but most notably in spot 1 at 5.7 atomic % could be because that iron can act as a grain refiner in Mg-Zn alloys, promoting the formation of fine and homogeneous grain structures as highlighted by (Jiang et al., 2020, Loukil 2022). Spot type 3 with 0.92 atomic % Zn could be because of the elongated morphology could be developed features that are more prominent during aging, particularly when considering that the investigated specimen is overaged. During heating, the formation of secondary phases of Mg-Zn alloys can include numerous intermetallic phases not only zinc but also zirconium which also is identified in spot type 3, this is in alignment to the research by (Yuan et al., 2021).

The summary of the identified elements and their atomic % for different zinc concentration and processing of Mg alloys show that some identified elements could be considered as outliers. These could be due to that they do not exist in the specimens or that they happened to be identified once for once particular spot type but not in the same spot type for another specimen. Contamination of Na which only is find for Mg low Zn extruded could occur from laboratory equipment, specimen preparation, exposure to the environment during storage of handling the specimens. Another one could be argon (Ar) which only is detected only for the overaged Mg medium Zn homogenized in table 5 opposed to table 6 or table 7 which suggest that it could be an outlier. However, another argument that contradicts my statements is that the noteworthy difference between overaged Mg medium Zn homogenized and the Mg medium Zn homogenized is that the material argon is detected. The reasoning behind why argon is exposed on the surface most likely has to do with the etching machine for ion polishing which requires argon in form of a gas. The ion polishing was not used for the other specimen, hence why argon could be detected. Spot type 3 in table 7 for the dark elongated morphology that most likely are microstructural features that develops during processing and aging explains why the Zr and Ca are identified since (Yang et al., 2008) mention that Zr and Ca are involved in the formation of intermetallic or compounds that segregate to or from the surface layer during the aging process which enhances precipitates. Aging also leads to changes in grain stricture and recrystallization, especially in the presence of alloying elements that can affects grain boundary stability such as Fe and Cu that diffuse more deeply into the bulk material or migrate toward the surface (Jo et al., 2020, Jiang et al., 2020), hence why these materials are found in table 5,6 and 7.

However, the Zn concentration increases the tolerance limits of impurities of Fe, Cu, Ni which enhances the corrosion resistance, this is stressed in the publication by (Jiang et al., 2020) and thereby make the results more reasonable. Similar trends regarding Ca and Zr on the Mg-Zn alloying surface were find in the report by (Jiang et al., 2020) highlighting that Ca forms compounds with elemental impurities and that Zr is considered to behave as an effective grain refiner.

The obtained result from SEM presents precipitates which are marked in red with circles and found in the following figures 32-27. The discovery of precipitates is also found in another aging experimental research documented by (Clark 1965, Chun et al., 1969, Mima et al., 1971, Wei et al., 19996). Initially upon aging, Mg-Zn alloys form GP-zones that are coherent clusters enriched in zinc. The zones are the earliest form or precipitates and contributes to

hindering dislocation movement. This could be whats shown in figure 32c) for Mg medium Zn homogenized, figure 34c) and figure 34d) for Mg high Zn extruded and figure 36c) and figure 36d) for Mg low Zn extruded as similar explanation is given by (Clark, 1965). As the aging progresses, precipitates are more recognizable and grow with characteristics of incoherent size that increases the hardening due to precipitation transition phase of β in the following sequence 110 °C, SSSS → pre β´- β´- β´´- β (Mg-Zn). This explanation by (Clark, 1965, Mima et al., 1971) is parallel with the results obtained in figure 35c), figure 35d) and figure 37a) and figure 37b) since the precipitates are more visible and larger during overaged stage. The quantity, size and distribution of the bright particles as precipitates also increases with more zinc concentration due to its influence on in accelerating the precipitation kinetics, thus making the material harder as described by the (Nie, 2012, Buha, 2008, Cheng et al., 2023). However, this argument is not aligned with the results for Mg extruded low Zn in figure 34d) and Mg extruded high Zn 35d) since the extruded specimen for the lower zinc concentration resulted in a higher hardness although the extruded high Zn is prone to show more precipitates, the reason behind this is that the precipitates are incoherent and does not affect the hardness. Another reason behind this could be the extrusion, but more experiments need to be conducted to confirm this.

(Smallman et al., 1999) shed lights on a phenom called particle coalescence which is a terminology for individual particles or cluster merge together to form larger particles. This can happen through atomic diffusion of zinc during the aging process where precipitates form and grow. The coalescence particles could be the explanation to the bigger particles that mostly sits around the grain boundary in figure 34d), 35d), 36d) and 37b).

Although precipitates improve mechanical strength, they adversely affect the corrosion as well. This statement is supported by the findings in the result of the extruded indentation when glancing through figure 24, 26 and 28. Despite the hardness increase, while looking at the surface surrounding the indentations, pitting corrosion and an ununiformed surface is found, particularly in figure 24a), 24b), 24c) and in figure 28a), 28b), 28d). The corrosion noticed on the surface is due the specimen reacting with other substances like oxygen or dirt, which much like could be the case during procedure of taking the specimen out of the oil bath, washing it with ethanol, drying it with compressed air and covering it with paper. Besides, magnesium vigorously reacts with oxygen which could be a contributing factor to why observation of corrosion was detectible.

5.3. Grain size analysis

Published work from (Tong et al., 2013, Zhang et al., 2011) shed light on how the extrusion process changes the materials characteristics, especially the grain boundary which have a direct effect on the material hardness due to more grain boundaries but of smaller sizes hinders dislocation movement and thereby increases the hardness. This explanation aligns well when comparing the grain sizes of the Mg medium Zn homogenized surface in figure 39 and figure 41 opposed to the extruded grain sizes in figure 43, 45, 47 and 49. Homogenized specimen surface have larger grain size and less spread of particles compared to extruded specimen surface with smaller grain size and where particles sit around the grain boundary. These results are consistent with expectations and corresponds to the emphasized information regarding grain sizes, homogenization and extrusion by (Callister et al., 2018, Smallman et al., 1999).

There is a noteworthy change in grain size with regards to before and after aging. This is most noticeable in figure 39 compared to figure 41, figure 43 compared to figure 45 and figure 47 compared to figure 49. The grain sizes obtained in the overaged stage in figures 42, 46 and 50 are smaller but in a larger quantity compared to the grain sizes in figure 40,44 and 48. The experimental results also confirms that the hardness in overaged condition is superior to the hardness at initial condition. Thus, there is a correlation between grain size and hardness.

When studying the values for mean intercept length, it enhances the understanding whether the material is prone to be harder. The smaller mean intercept length usually means that the material is harder. This statement can be backed by comparisons of mean intercept length of 6.1 μm for Mg high Zn extruded compared to 5.6 μm overaged Mg high Zn extruded. Additionally, the prerequisites remain the same for mean intercept length for Mg low Zn extruded being 6 μm compared to mean intercept length of overaged Mg low 5.4 μm. However, this seems also be the case since the statement in terms of intercept length being prone to hardness is also argued for with the results for the mean intercept length from Mg medium Zn homogenized is 39 μm while overaged Mg medium Zn resulted is 31 μm. With regards to another contributing aspect worth considering is that the 7 horizontal lines through the surface could happen to not cross a region where not many grain boundaries appeared which then would affect the calculations for the mean intercept length.

6. Conclusions

In this work, three Mg-Zn based alloys with varying concentrations of Zn supplied in as-homogenized and as-extruded conditions were aged at 180°C for up to 26 hours. During the aging treatment, specimens were extracted at regular time intervals for hardness measurements. As a result, peak-aged time was found along with maximum hardness values for each sample. Following microscopic analysis allowed making the following conclusions about the correlation between the material characteristics and their microstructures.

In the as-supplied homogenized state, the alloy with medium concentration of Zn has the lowest hardness of 53.5 HV, while high-Zn intermediate and low-Zn the highest hardness of 63.8 HV. This difference is substantial but not large, and considering rather high variation of hardness within each sample, it can be deemed statistically insignificant. Therefore initial hardness in the alloys under investigation can be concluded to have a low dependence on the quantity of Zn. By contrast, the kinetics of aging suggests significant dependence of investigated alloys on Zn concentration. In the peak-aged condition, hardness is lowest in the low-Zn alloy at 68.6 HV increasing monotonically to the highest value of 74 HV in the high-Zn alloy, which is a typical dependence in such age-hardenable alloys. The analysis of microstructure in SEM did not reveal significant changes in grain sizes and primary precipitate structure during ageing. Knowing that secondary precipitates are beyond the resolution of SEM used in this study, we can attribute the increase of hardness to the formation of secondary precipitates remaining small and (semi-)coherent to the Mg matrix.

In the as-supplied extruded state, the alloy with medium concentration of Zn has the highest hardness of 66.1 HV, while low-Zn intermediate and high-Zn the lowest hardness of 61.9 HV. Similar to the as-homogenized state, this difference is not large, and even considering lower variation within each sample, it can still be deemed statistically insignificant and therefore having a low dependence on the quantity of Zn. By contrast to the homogenized state, aging leads to rather modest increase in hardness to 65.0 HV in high-Zn, 69.6 HV in medium-Zn, and 72.5 HV in low-Zn alloys. The analysis of microstructure in SEM revealed significantly lower grain sizes compared to the homogenized material but no significant difference in grain sizes between different alloys in both as-extrudeded and as peak-aged coniditions. By contrast, major difference were found in the primary precipitate structure. Even in the as-supplied conditoin, both the extruded alloys showed large number density of incoherent primary precipitates rather homogenously distributed within the matrix. The ageing treatment led to noticable coarsening of these precipitates and their segregataion at grain boundaries. Therefore, we can conclude that in the extruded alloys, hardness is primarily controlled by grain structure and to a lesser extent by incoherent precipitates.

The maximum hardness values after aging of homogenized alloys were similar to those in the extruded counterparts. This suggests that processing technologies controlling grain sizes and precipitate structure can be efficient for optimising material performance. Further prioritisation of hardness control option can be made based on other performance characteristics, e.g. such as degradatoin rate in the case of biomedical applicatoins, or processing technology avaliable at a material fabricatoin facility.

7. Future work

The result gathered in this work invites further analysis.

The performed analysis would benefit from a larger data set in hardness test as only 11 tests were made for every hour, this would lead to more accurate data and not much spread but would require longer time during the hardness tester which already is time consuming.

Since this experiment is carried out with 180 °C, same experiment could be carried out in different temperatures such as 150°C and 100 °C to further investigate and analyze the aging kinetics and compare the affecting parameters as this would be of interest. Additionally, longer aging time along with hardness test after couple of hours but the other prerequisites remain the same would be beneficial to see how both temperature and time will affect the hardness for different processing of Mg alloys of Mg-Zn alloys with different alloying composition of Zn.

The mechanisms behavior of Mg-Zn alloys are of interest to fully understand how hardness is affected during aging. To study this, multiple tests of hardness must be performed in different temperatures and Zn concentration to acquire a profound and in-depth knowledge of precipitation kinetics of Mg-Zn alloys. This will also help the fields of biomedical magnesium.

8. References

Abbaschian, R., Abbaschian, L., Reed-Hill, R. E. (2009). Physical metallurgy principles. Cengage Learning, 4th ed. SBN-10: 0-495-08254-6

Askeland, D.R., Fulay, P.P., Wright, W.J. (2010). The Science and Engineering of Materials. Cenagle Learning, 6th ed. ISBN-10: 0495296023.

ASM International Handbook Committee. (1991). Heat treating. Vol.4. ISBN-10: 0871703793 http://products.asminternational.org/hbk/do/navigate?navOn=true&src=/content/V04/D00/A01/index.htmln

ASM International., Baker, H., Henry, S. D., Okamoto, H. (1992). Alloy Phase Diagram. ASM handbook. Vol. 3. ISBN: 9780871703811

Asadollahi, M., Gerashi, E., Alizadeh, R., Mahmudi, R. (2022). Effect of Zn content and processing route on the microstructure, mechanical properties, and biodegradation of Mg–Zn alloys. Journal of Materials Research and Technology, Volume 21, p 4473-4489. https://doi.org/10.1016/j.jmrt.2022.11.041.

Biotronik AG, https://www.biotronik.com/en-de/products/coronary/magmaris [Accessed 2024- 04-23]

Buha, J. (2008).Reduced temperature (22–100 °C) ageing of an Mg–Zn alloy. Materials Science and Engineering; A,Volume 492, Issues 1–2, 11-19, ISSN 0921-5093. https://doi.org/10.1016/j.msea.2008.02.038

Buha, J., Ohkubo, T. Natural Aging in Mg-Zn(-Cu) Alloys. (2008). Metall Mater Trans A 39, 2259–2273. https://doi.org/10.1007/s11661-008-9545-y

Callister, W.D., Rethwisch, D.G. (2018). Materials Science and Engineering: An Introduction. Wiley, 10th ed. ISBN-13: 9781119321590

Cha, J.W., Jin S.C., Jung, J.C., Park, S.Y. (2022). Effects of homogenization temperature on microstructure and mechanical properties of high-speed-extruded Mg–5Bi–3Al alloy. Journal of Magnesium and Alloys.Volume 10, Issue 10,p 2833-2846. https://doi.org/10.1016/j.jma.2021.07.007.

Chapuis, A., Driver J.H. (2011). Temperature dependency of slip and twinning in plane strain compressed magnesium single crystals. Acta Materialia, vol. 59, p. 1986–1994. https://doi.org/10.1016/j.actamat.2010.11.064

Cheng, D., Wang, K., Zhou, B-C. (2023). Crystal structure and stability of phases in Mg-Zn alloys: A comprehensive first-principles study,Acta Materialia. Volume 242. https://doi.org/10.1016/j.actamat.2022.118443.

Chun, J.S., Byrne, J.G. (1969). Precipitate strengthening mechanisms in magnesium zinc alloy single crystals. J Mater Sci 4, 861–872. https://doi.org/10.1007/BF00549777

Clark, J.B. (1965). Transmission electron microscopy study of age hardening in a Mg-5wt.% Zn alloy. Acta Metallurgica,Volume 13, Issue 12, p 1281-1289. https://doi.org/10.1016/0001-6160(65)90039-8.

Clark, J.B., Zabdyr, L., Moser, P. (1988). Phase Diagrams of Binary Magnesium Alloys, ASM International, Metals Park, OH, 353-364.

Du, Z., Wang, D., Zhang, W. (1999). J. Alloys Compounds. Vol. 284, pp. 206–12.

Egerton, R.F. (2005). Physical principles of electron microscopy: An introduction to TEM, SEM, and AEM. Springer Cham, 2nd ed. https://doi.org/10.1007/978-3-319-39877-8

Esmaily, M., Svensson, J., Fajardo, S., Birbilis, N., Frankel, G., Virtanen, S., Arrabal, R., Thomas, S., Johansson, L. (2017). Fundamentals and advances in magnesium alloy corrosion. Progress in Materials Science, vol. 89, 2017, pp.92-193. https://doi.org/10.1016/j.pmatsci.2017.04.011

Espiritu, J., Berangi, M., Yiannakou, C., Silva, E., Francischello, R., Kuehne, A., Niendorf, T., Könneker, S., Willumeit-Römer, R., & Seitz, J. M. (2022). Evaluating metallic artefact of biodegradable magnesium-based implants in magnetic resonance imaging. Bioactive materials, 15, 382–391. https://doi.org/10.1016/j.bioactmat.2021.11.035

Frost H. M. (1994). Wolff's Law and bone's structural adaptations to mechanical usage: an overview for clinicians. The Angle orthodontist, 64(3), 175–188. https://doi.org/10.1043/0003-3219(1994)064<0175:WLABSA>2.0.CO;2

Geetha, B., Ganesan, K. (2015). The Effects of Ageing Temperature and Time on Mechanical Properties of A356 Aluminium cast Alloy with Red Mud Addition and Treated By T6 Heat Treatment. Materials Today: Proceedings, Volume 2, Issues 4–5, p1200-1209. https://doi.org/10.1016/j.matpr.2015.07.032.

Goldstein, J.I., Newbury, D.E., Joy, D.C., Lyman, C.E., Echlin, P., Lifshin, E., Sawyer L., Micheal, J.R. (2003). Scanning Electron Microscopy and X-Ray Microanalysis. Kluwer Academic, Plenum Publishers, 3rd ed. https://doi.org/10.1007/978-1-4615-0215-9

Hambidge, M. (2000). Human zinc deficiency. The Journal of nutrition, 130(5S Suppl), 1344S–9S. https://doi.org/10.1093/jn/130.5.1344S

Hare, D. J., New, E. J., De Jonge, M. D., McColl, G. (2015). Imaging metals in biology: Balancing sensitivity, selectivity and spatial resolution. Chemical Society Reviews. https://doi.org/10.1039/C5CS00055F

Hassan, S.F., Islam, M.T., Saheb, N., Baig, M.M.A. (2022). Magnesium for Implants: A Review on the Effect of Alloying Elements on Biocompatibility and Properties. Materials 15, no. 16: 5669. https://doi.org/10.3390/ma15165669

Hegazy, R., Aswal, D.K., Yadav, S., Takatsuji, T., Rachakonda, P., Kumar H. (2023). Hardness Metrology: Hnadbook of Metrology and Applications. ISBN978-981-99-2073-0. https://doi.org/10.1007/978-981-99-2074-7_41

Henkel, D.P., Pense, A.W. (2001). Structure and Properties of Engineering materials. McGraw-Hill, 5th ed. ISBN: 9780072350722.
Hermawan, H. (2012). Biodegradable Metals: From Concept to Applications. SpringerBriefs in Materials, p 13-19. ISBN 978-3-642-31169-7. https://doi.org/10.1007/978-3-642-31170-3

Hollerith, C., Wernicke, D., Bühler, M., Feilitzsch, F. v., Huber, M., Höhne, J., Hertrich, T., Jochum, J., Phelan, K., Stark, M., Simmnacher, B., Weiland, W., Westphal, W. (2004). Energy dispersive X-ray spectroscopy with microcalorimeters. Nuclear Instruments and Methods in Physics Research Section A: Accelerators, Spectrometers, Detectors and Associated Equipment. Volume 520, Issues 1–3, p 606-609. https://doi.org/10.1016/j.nima.2003.11.327.

Huang, H., Yuan, G., Chu, Z., Ding, W. (2013). Microstructure and mechanical properties of double continuously extruded Mg–Zn–Gd-based magnesium alloys. Materials Science and Engineering A. 560. 10.1016/j.msea.2012.09.063.

Humphreys, F.J. and Hatherly, M. (2004).Recrystallization and Related Annealing Phenomena. 2nd Ed, Elsevier Science Ltd., Pergamon. https://doi.org/10.1016/B978-0-08-044164-1.X5000-2

Jiang, P., Blawert, C., & Zheludkevich, M. L. (2020). The Corrosion Performance and Mechanical Properties of Mg-Zn Based Alloys—A Review. Corrosion and Materials Degradation, 1(1), 92– 158. MDPI AG. http://dx.doi.org/10.3390/cmd1010007

Jo, S., Whitmore, L., Woo, S., Aramburu A.U., Letzig, D., Yi, S. (2020). Excellent age hardenability with the controllable microstructure of AXW100 magnesium sheet alloy. Sci Rep 10, 22413. https://doi.org/10.1038/s41598-020-79390-z

Kaya, A.A., Pekguleryuz M., Eliezer, D. (2005). High temperature deformation, alloys and processing of magnesium, in The Deformation and Processing of Structural Materials, pp. 29-30. https://doi.org/10.1533/9781845690786.29

Kirkland, N.T., Birbilis, N. (2014). Magnesium Biomaterials: Design, Testing, and Best Practice. Springer. ISBN-10 9783319021225. https://link.springer.com/book/10.1007/978-3-319-02123-2

Leng, Y. (2013). Materials characterization: introduction to microscopic and spectroscopic methods. Wiley- VCH Verlag GmbH & Co;, 2nd ed. ISBN:9783527670772. DOI:10.1002/9783527670772

Liang, H., Dong, Z., Zhang, Y., Bai, Y. (2023). Homogenization treatment and heat deformation behavior of cast ZK60 magnesium alloy. J. Phys.: Conf. Ser. 2459. doi:10.1088/1742-6596/2459/1/012038

Liu, R.; Wang, J.; Wang, L.; Zeng, X.; Jin, Z. (2022). Cluster Hardening Effects on Twinning in Mg-Zn-Ca Alloys. Meteals no. 4: 693. https://doi.org/10.3390/met12040693

Liu, S., Esteban-Manzanares, G., & LLorca, J. (2020). First-principles analysis of precipitation in Mg-Zn alloys. Physical Review Materials, 4(9), 093609. https://doi.org/10.48550/arXiv.2009.01892

Liu W, Zhang C, Shi Q, Han F, Cao P. (2024). Dynamic Recrystallization, Texture Evolution, and Improved Mechanical Properties of Mg-Y-Zn-V Alloy during Forging and Subsequent Extruding Deformation. Metals, 14(3):259. https://doi.org/10.3390/met14030259

Liu, X., Yin, M., Zhang, S., Wei, H., Liu, B., Du, H., Hou, L. and Wei, Y. (2018). Corrosion Behavior of the As-Cast and As-Solid Solution Mg-Al-Ge Alloy. Materials, 11(10), p.1812. https://doi.org/10.3390/ma11101812

Loukil, N. (2022). Alloying Elements of Magnesium Alloys: A Literature Review. IntechOpen. http://dx.**doi**.org/10.5772/**intechopen**.**96232**

Mandia, R. (2018). On the deformation behavior of Magnesium bicrystals at room and elevated temperature: Compression test parallel to the c-axis

Mima, G., Tanaka, Y. (1971). The Aging Characteristics of Magnesium-4wt% Zinc Alloy. Transactions of the Japan Institute of Metals. Volume 12, Issue 2, p 71-75 https://doi.org/10.2320/matertrans1960.12.71

Nie, JF. (2012). Precipitation and Hardening in Magnesium Alloys. Metall Mater Trans A 43, 3891–3939. https://doi.org/10.1007/s11661-012-1217-2

Okamoto, H., Massalski, T.B. (1993). J. Phase Equilibrium. Vol. 14 (3), pp. 316–35.

Pekguleryuz, M.O., Kainer, K., Kaya, A.A. (2013). Fundamentals of Magnesium Alloy Metallurgy. Woodhead publishing. ISBN 978-0-85709-088-1.

Philips (1996). Environmental Scanning Electron Microscopy – An introduction to ESEM. Chapter 2 SEM-basics. Eindhoven: Philips Electron, Optics; 2nd ed.

Polmear, I., StJohn, D., Nie, J.F., Qian, M. (2017). Light alloys: Metallurgy of the light metals (5th ed.). Elsevier. pp 287 – 367, ISBN 978-08-099431-4.

Prasand B., Bhingole, P. (2017). Critical assessment of strengthing mechnincsm of magnesium alloys: Review. https://doi.org/10.5185/amp.2017/859

PubChem, National Center for Biotechnology Information (2024). Magnesium Oxide. [Accessed 2024- 04-29. https://pubchem.ncbi.nlm.nih.gov/compound/Magnesium-Oxide.

Smallman, R.E., Bishop, R.J. (1999). Modern Physical Metallurgy. Elsevier, 6th ed. ISBN 978-0-7506-4564-5. https://doi.org/10.1016/B978-0-7506-4564-5.X5000-9

Soboyejo, W. (2002). Mechanical Properties of Engineered Materials (1st ed.). CRC Press. https://doi.org/10.1201/9780203910399

Somekawa, H., Osawa, Y., Mukai, T. (2006). Effect of solid-solution strengthening on fracture toughness in extruded Mg–Zn alloys. Scripta Materialia,Volume 55, Issue 7. Page593-596. https://doi.org/10.1016/j.scriptamat.2006.06.013.

Staiger, M., Pietak, A., Huadmai, J. and Dias, G. (2006). Magnesium and its alloys as orthopedic biomaterials: A review. Biomaterials, 27(9), pp.1728-1734. https://doi.org/10.1016/j.biomaterials.2005.10.003

Struers. Selection guide for cutting wheels. https://www.struers.com/en/Products/Cutting# [Accessed 2024-04-24].

Syntellix A.G., https://www.syntellixA.G.de/en/products/product-overview/all.html [Accessed 2024-04-23]

Tan, J., Ramakrishna.S. (2021). Applications of Magnesium and Its Alloys: A Review. Applied Sciences 11, no. 15: 6861. https://doi.org/10.3390/app11156861

Tong, L.B., Zheng, M.Y., Cheng, L.R., Kamado, S., Zhang, H.J. (2013). Effect of extrusion ratio on microstructure, texture and mechanical properties of indirectly extruded Mg–Zn–Ca alloy. Materials Science and Engineering: Volume 569, p 48-53. https://doi.org/10.1016/j.msea.2013.01.052.

Ren, Y., Liu, B., Xie, H., Li, H., Jiang, M., Qin, G. (2021). Characterization of precipitates in aged Mg-4 wt%Zn alloy. Materials Today Communications,Volume 26. https://doi.org/10.1016/j.mtcomm.2021.102017.

Roh, HJ., Park, J., Lee, SH. et al. (2022). Optimization of the clinically approved Mg-Zn alloy system through the addition of Ca. Biomater Res **26**, 41. https://doi.org/10.1186/s40824-022-00283-5

Viklund, M. (2019). Degradation of model biomedical Mg alloys in aqueous media. Master Thesis at Lund University.

Vinogradov, A., Merson, E., Myagkikh, P., Linderov, M., Brilevsky, A., Merson D. (2023). Attaining High Functional Performance in Biodegradable Mg-Alloys: An Overview of Challenges and Prospects for the Mg-Zn-Ca System. Materials; 16(3):1324. https://doi.org/10.3390/ma16031324

Wei, L.Y., Dunlop, G.L., Westengen, H. (1996). Age hardening and precipitation in a cast magnesium-rare-earth alloy. J Mater Sci 31, 387–397. https://doi.org/10.1007/BF01139156
Wei, L.Y., Dunlop, G.L. & Westengen, H. (1996). Precipitation Hardening of Mg-Zn and Mg-Zn-RE alloys. Metall Mater Trans A 26, 1705–1716 . https://doi.org/10.1007/BF02670757

Witte, F. (2015) Reprint of: The history of biodegradable magnesium implants: A review. Acta Biomaterialia 23, Supplement, S28-S40. https://doi.org/10.1016/j.actbio.2010.02.028

Xu S.W., Oh-ishi, K., Sunohara, H., Kamado, S. (2012).Extruded Mg–Zn–Ca–Mn alloys with low yield anisotropy. Materials Science and Engineering: A. Volume 558, p 356-365, https://doi.org/10.1016/j.msea.2012.08.012.

Zeng, Z., Stanford, N., Davies, C. H. J., Nie, J. F., & Birbilis, N. (2019). Magnesium extrusion alloys: a review of developments and prospects. International Materials Reviews, 64(1), 27–62. https://doi.org/10.1080/09506608.2017.1421439

Zhang, T., Shao, Y. Meng, G. Cui, Z. Wang, F. (2011). Corrosion of hot extrusion AZ91 magnesium alloy: I-relation between the microstructure and corrosion behavior. Corrosion Science,Volume 53, Issue 5,p 1960–1968.https://doi.org/10.1016/j.corsci.2011.02.015.

Zhao, D., Wang, Z., Zuo, M., Geng, H. (2014). Effects of heat treatment on microstructure and mechanical properties of extruded AZ80 magnesium alloy. Materials and Design (1980-2015). Volume 56, p 589-593. https://doi.org/10.1016/j.matdes.2013.11.072.

Yuan J, Li T, Zhang K, Li X, Li Y, Ma M, Shi G, Du Z, Liu W, Peng Y. (2021). Precipitation Behavior of Mg-7Gd-3Y-2Zn-0.5Zr Alloy during Isothermal Aging. Materials 14(7):1737. https://doi.org/10.3390/ma14071737

Yang, Z., Li, J., Zhang, J., Lorimer, G., Robson, J. (2008). Review on research and development of magnesium alloys. Acta Metall. Sin., 21, 313–328. https://doi.org/10.1016/S1006-7191(08)60054-X

Appendix 1 – EDS diagram and table composition

The diagrams and table compositions found in figure A1.1 is from spot type 1 analyzed from Mg low Zn extruded from figure 38.

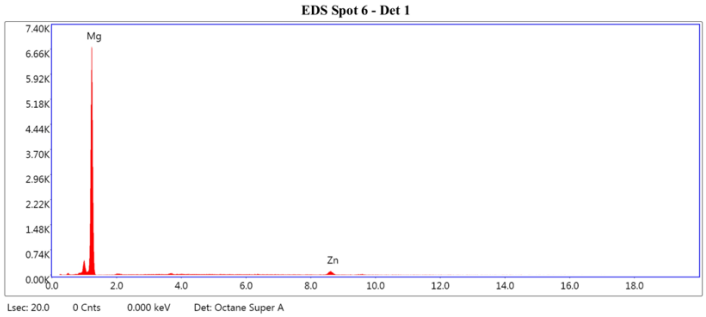

Element	Weight %	Atomic %	Net Int.	Error %	Kratio	Z	A	F
MgK	87.02	94.74	2579.02	4.84	0.5840	1.0238	0.6554	1.0001
ZnK	12.98	5.26	79.71	8.94	0.1134	0.8136	1.0066	1.0666

Figure A1.1: EDS diagram and table composition of spot type 1 for Mg low Zn extruded.

The diagrams and table compositions found in figure A1.2 is from spot type 2 analyzed from Mg medium Zn homogenized.

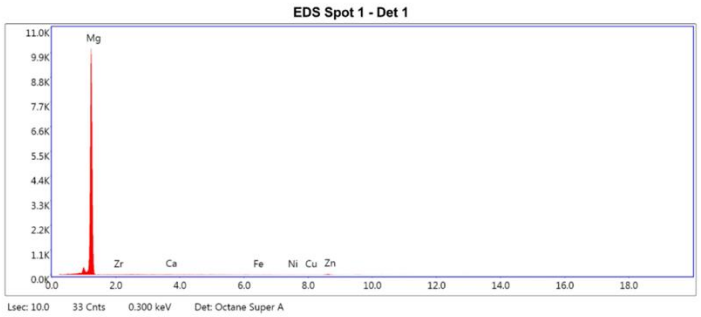

Element	Weight %	Atomic %	Net Int.	Error %	Kratio	Z	A	F
MgK	96.35	98.57	7744.13	2.44	0.8596	1.0064	0.8865	1.0001
ZrL	0.08	0.02	1.44	70.34	0.0004	0.7640	0.6451	0.9987
CaK	0.15	0.10	5.78	69.38	0.0013	0.9363	0.8957	1.0152
FeK	0.14	0.06	3.29	67.16	0.0013	0.8352	0.9978	1.1007
NiK	0.11	0.05	2.23	75.98	0.0011	0.8429	1.0044	1.1602
CuK	0.18	0.07	2.98	70.32	0.0017	0.7998	1.0061	1.1772
ZnK	2.99	1.14	39.36	18.92	0.0274	0.7971	1.0072	1.1435

Figure A1.2: EDS diagram and table composition of spot type 2 for Mg medium Zn homogenized.

The diagrams and table compositions found in figure A1.3 is from spot type 3 analyzed from overaged Mg medium Zn homogenized.

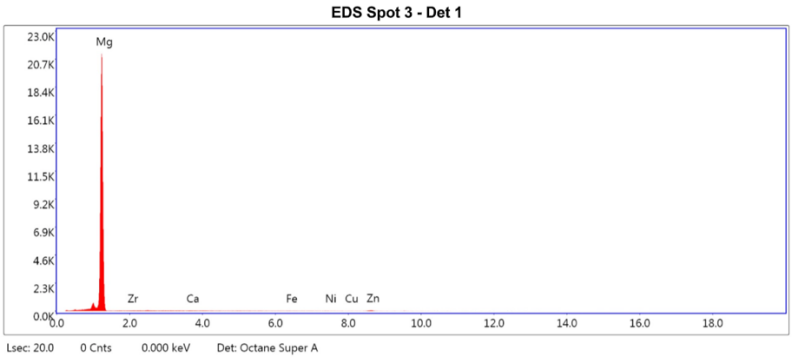

Element	Weight %	Atomic %	Net Int.	Error %	Kratio	Z	A	F
MgK	96.48	98.61	8336.73	2.23	0.8679	1.0061	0.8941	1.0001
ZrL	0.15	0.04	2.94	49.69	0.0007	0.7637	0.6462	0.9987
CaK	0.20	0.12	7.94	61.82	0.0017	0.9360	0.8959	1.0151
FeK	0.21	0.09	5.23	61.22	0.0019	0.8349	0.9978	1.0988
NiK	0.22	0.09	4.61	64.92	0.0022	0.8426	1.0043	1.1544
CuK	0.11	0.04	1.82	68.77	0.0010	0.7995	1.0059	1.1744
ZnK	2.64	1.00	37.20	15.95	0.0243	0.7968	1.0069	1.1479

Figure A1.3: EDS diagram and table composition of spot type 3 for overaged Mg medium Zn homogenized.